IP-BBSR-9341

Fermilab Library

0 1160 0031848 9

IP/BBSR/93-41

August '93

# RAMAN SCATTERING IN A CORRELATED SUPERCONDUCTOR II A FINITE TEMPERATURE STUDY[1]

Debanand Sa[2] and S. N. Behera

Institute of Physics, Bhubaneswar-751005, INDIA

[1] A preliminary account of this work was presented at the "International Symposium on Local Order in Condensed Matter Physics" held at Jekyll Island, Georgia, USA, during June 14-17, 1993

[2] e-mail:debanand@iopb.ernet.in

**Abstract**

The temperature dependence of the Raman spectrum of copper oxide superconductors is calculated assuming that the normal state of these systems is a correlated metal and that the superconductivity arises due to the correlation bag mechanism as proposed earlier [3] (here after referred to as I). The correlated metallic state is characterised by the presence of a strong interaction between the doped charge carriers and the quanta of fluctuations of the resonating valence bonds present in the normal state. It is shown that the presence of such an interaction gives rise to the marginal Fermi liquid behaviour, associated with the pair polarisability function. The model therefore, successfully explains the constant intensity background observed in the Raman spectrum due to the scattering by the charge carriers. In order to understand the observed temperature dependent shift and change in width of the phonons, their spectral density functions are calculated. Two different kinds of interaction between the charge carriers and phonons were derived in I. One corresponding to the usual electron-phonon interaction where a phonon decays by exciting an electron-hole pair and the other where the decay process involves a quasi particle pair. It was postulated that the localised phonons couple to the charge carriers by the later process where as the propagating ones interact by the former. The temperature dependence of the phonon self energies due to the two processes is calculated and the spectral density functions are computed. The calculated temperature dependent shift and change in width of the phonons show qualitative agreement with the observed result.

Keywords: correlated metallic state, response functions, high temperature superconductivity, electron-phonon interaction, Raman scattering.



# 1 Introduction

Raman scattering in the cuprate superconductors [1] has shown several unusual features in the normal state as well as in the superconducting state. In the normal state, a rather large but constant background intensity has been observed at all frequencies up to the highest measured frequency which has been attributed to the scattering by the charge carriers [2] in the system. Three prominent phonon peaks having frequencies of $116cm^{-1}$, $340cm^{-1}$ and $504cm^{-1}$ ride over the constant background intensity out of which some show Fano line shape indicating a strong coupling to the charge carriers in the system. On lowering the temperature below the superconducting transition temperature ($T_c$), the constant background intensity is suppressed at low frequencies which may be taken as a signature of the opening of a superconducting gap in the system. Furthermore, there appears a broad peaking of the intensity at a higher frequency, with the indications that this peak may also be a normal state feature. Moreover, some of the phonons show anomalous softening while others harden on lowering the temperature below $T_c$, accompanied by a broadening or narrowing of their linewidths. A detailed summary of these results has already been presented in an earlier paper [3] (here after referred as I). However, more recently the results of some measurements have appeared in the literature which focus the attention (i) on the shift and width of phonons as a function of the charge carrier concentration [4] and (ii) on the temperature and carrier concentration dependence of the Raman scattering constant intensity background [5, 6]. A more careful analysis of the Raman data indicated that the temperature dependence

of some of the Raman active phonons in the cuprates are very much sensitive to the oxygen content as shown recently by Altendorf et al [4] from their measurement on $YBa_2Cu_3O_\delta$. They studied the temperature dependence of the $340cm^{-1}$ and $440cm^{-1}$, $500cm^{-1}$ phonon in different crystals of $YBa_2Cu_3O_\delta$ ($6.7 \leq \delta \leq 7.0$). The samples which they used are denoted as $A, B, C, D, E, F$ and $G$ with the corresponding oxygen concentrations $7.0, 6.99, 6.93, 6.90, 6.86, 6.81$ and $6.68$ and transition temperatures $89.7, 92.8, 93.7, 92.0, 91.1, 87.7$, and $59.2$ K respectively. A brief summary of the main features in their experiments are as follows: On reducing the temperature through $T_c$, the $340cm^{-1}$ phonon show softening in all the crystals, the largest being in the oxygeneted sample $A$ and the degree of softening reduces as the oxygen concentration decreases, vanishing in the crystal $G$ while its linewidth narrows in $C, D, E$ and $F$ but broadens in $A$ and $B$. On the otherhand, the $440cm^{-1}$ and $500cm^{-1}$ phonons harden in all the crystals except $G$ below $T_c$. The degree of hardening decreases as the oxygen concentration decreases being largest in the crystal $A$ but the frequency of the $440cm^{-1}$ phonon softens marginally in the deoxygeneted sample $G$. Moreover, the $500cm^{-1}$ phonon show softening in the sample $G$, at a temperature of approximately 50 K which is well above the $T_c$ of that sample. This may be a signature of the appearence of a gap in the normal state. Moreover, the linewidth broadens in the crystals $A, B$ and $C$ and it becomes diminished in the samples $D, E$ and $F$ but narrows down in $G$ below $T_c$. In the case of the $340cm^{-1}$ phonon, the phonon peaks become more symmetric on decreasing the oxygen concentration suggesting that there may be a reduction in the strength of interaction



of the $340cm^{-1}$ phonon with the charge carriers in the deoxygeneted samples. In contrast, in the case of $440cm^{-1}$ and $500cm^{-1}$ phonons, the peaks are symmetric in crystals $A, B, C, D, E$ and $F$ while asymmetric in $G$ which implies that the interaction of the phonons to the charge carriers becomes strong in the deoxygeneted samples compared to the oxygeneted ones. From the above data, it is obvious that these two different sets of phonons show quite opposite behaviour to each other and hence may be concluded that the $440cm^{-1}$ and the $500cm^{-1}$ phonons interact with a different set of electrons than does the $340cm^{-1}$ phonon. While the above measurements focus on the scattering by phonons, the experiment of Maksimov et al [5] and that of Sugai et al [6] dealt with the Raman scattering by the charge carriers. Again the later measurements were carried out on different samples of $YBCO$ with varying oxygen content using polarised light. The note worthy features of these measurements are (i) the observation of a gap anisotropy in the superconducting state and (ii) the appearence of a constant intensity background in the normal state even in the insulating samples. It was inferred that the later behaviour is different from the intensity due to the charge carrier scattering in the metallic state. This led to the conclusion that the Raman scattering in the metallic and insulating samples are caused by different charge carriers. Similar results on the $La_{2-x}Sr_xCuO_4$ samples have been reported by Sugai et al [6].

It is worth while to analyse the new results in terms of the model for Raman scattering proposed by us in I. Besides, in I we confined our selves only to a zero temperature calculation of the Raman intensities arising from the scattering by phonons alone. In

this paper we generalise the work (i) by including the scattering by the charge carriers and (ii) by performing a finite temperature calculation. A brief summary of the model of the normal and the superconducting states proposed in I is given below:

A model for the normal state as well as the superconducting state was proposed by us in I to fecilitate the calculation of the phonon spectral density functions needed to explain the phonon anomalies observed in the Raman scattering experiments. The model evolves from the fact that the long range antiferromagnetic ordering of the basic insulating material gets suppressed on doping the system, resulting in a disordered, magnetic, insulating ground state which is taken to be the insulating RVB state. On further increasing the doping concentration, it was argued that because of the presence of excess holes in the system (when the doping concentration exceeds a critical value such that one crossses the insulator-metal boundary) the RVB metallic state is formed, where the elementary excitations are the regular fermions carrying both spin and charge. Unlike the BZA [7] picture, we further assume that this metallic state is characterised by the opening of a finite gap over the regions of the Fermi surface due to the presence of some singlet bonds in the system. However, simultaneously the presence of a relatively large number of holes will result in strong fluctuations in the singlet bonds and hence in the amplitude and the phase of the gap, the quanta of these fluctuations being the collective modes of the system. Due to the very nature of their origin these amplitude and the phase modes will interact rather strongly with the quasi particles of the RVB metallic state. This interaction of the quasi particles with the collective modes is the most important



feature which characterises the normal state of the system, we call the correlated metallic state. As a result of this interaction, the quasi particles acquire a self energy whose imaginary part gives a life time in accordence with the requirements of the marginal Fermi liquid theory. Hence this model for the normal state is capable of explaining the observed linear temperature dependence of the resistivity in the cuprates over a wide temperature range. The phase diagram of the cuprates in general and $La_{2-x}Sr_xCuO_4$ in particular shows that the range of dopant concentrations where superconductivity appears is also the range where the normal state is a bad metal. On increasing the dopant concentration beyond this range the material becomes a good Fermi liquid like metal, but does not become a superconductor on lowering the temperature even upto the lowest possible temperature available. This is in keeping with the general thumb rule that bad metals are good superconductors. Hence whatever is the mechanism that causes the high resistance in the normal state is also responsible for superconductivity. In the present model under consideration the resistance in the normal state is due to the scattering of the quasi particles by the collective modes. Hence superconductivity in these system must also be due to the pairing of the quasi particles brought about by an attractive interaction mediated by these collective modes. This is the so called correlation bag mechanism proposed by us in I in analogy with the spin bag model of Schrieffer et al [8]. While the later works in the weak correlation limit, the former arises when the correlations are strong.

As is well known, Raman scattering proceeds by polarising the medium, hence in

the metallic state the incident electro-magnetic radiation creates an electron-hole pair which recombine to give the scattered radiation. However, since the present model of the correlated metal consists of singlet bonds as well as the charge carriers, there will be an additional contribution to the polarisation coming from the possibility of breaking the bonds, as well. This polarisability will essentially be given by the pair polarisability function. Besides, the electron or hole can emit or absorb a phonon giving rise to inelastic scattering of the radiation because of the electron-phonon interaction inherent in the medium. Therefore, in order to calculate the Raman scattering amplitude, it is necessary to evaluate the phonon response of the system which will depend on the coupling of the phonons to the elementary excitations in the ground state. However, in the correlated metallic state that we proposed, there can exist two different mechanisms for the coupling of the phonons with the charge carriers as discussed in I. The first is the usual electron-phonon interaction mechanism arising from the modulation of the hopping integral ($t_{ij}$) due to the displacement of the ions from their equilibrium positions whereas the second could be due to the modulation of the exchange integral ($J_{ij}$) due to phonons. This later mechanism amounts to a coupling of the phonons to the charge carrier pairs in the correlated metallic state. These two different interaction mechanisms will modify the phonon spectrum in different ways. Because of the interaction of phonons with the charge carrier pairs, the pair amplitude mode is expected to show up in the Raman spectrum. Similarly due to the charged nature of the superconducting state, the density response function is expected to couple to the collective modes of the superconducting



state, therefore Raman spectrum is expected to show the signatures of these modes as well.

The rest of the paper is organised as follows: In section 2 we discuss the essentia processes for the calculation of the Raman intensities. The polarisabilities in the norma and the superconducting state are calculated in section 3 and 4 respectively. In sectior 5, the basic charge carrier-phonon interactions in the strongly correlated metallic stat are presented and the corresponding phonon Green's functions and their spectral densit functions are obtained at finite temperatures. The results and their comparision witl the experimental Raman data are presented in section 6. Finally, the main results o the paper are summarized in the concluding section 7.

## 2 Raman Intensity

The scattering of light in normal metals [11] proceeds as follows: The inciden photon excites an electron-hole pair, either of which emits or absorbs a phonon due t the electron-phonon interaction in the system. Finally, the electron and hole recombin giving rise to the scattered photons. Therefore, in such a process the scattered intensit of the photon will be proportional to the sum of the imaginary part of the particle hole polarisability (density response function) and the spectral density function for th phonons. But as discussed in the introduction, in the case of the cuprate superconductor the normal state differs from that of the usual metals. Therefore, the light scatterin process has to be modified. Due to the presence of the quasi particle pairs in th

normal state, the incident photon besides exciting the particle-hole pairs, can also break the local pairs which gives rise to the anomalous polarisability. Moreover, this process will also couple to the localised phonons in the system as discussed in I. Thus in the correlated metallic state, the Raman intensity will acquire an additional contribution coming from the sum of the imaginary part of the pair polarisability function and the spectral density function for the localised phonons. The expression for the Raman intensity $I(\omega)$ therefore, is given as

$$I(\omega) = (1 + n(\omega))[-Im\chi^{p-p}(0,\omega) - Im\chi^{p-h}(0,\omega) + \sum_{i=l,p} S^i(0,\omega)] \qquad (1)$$

where $n(\omega)$ is the Bose factor, $\chi^{p-p(p-h)}(0,\omega)$ being the polarisabilities in the particle-particle (particle-hole) channel, $S^i(0,\omega)$ is the phonon spectral density function for the propagating (p) and the localised (l) phonons. The polarisabilities and the spectral density functions for the phonons have to be calculated in both the normal state as well as the superconducting state to compute the Raman intensity.

# 3 The Response Functions in the Correlated Metallic State

The insulating RVB state resulting from the single band Hubbard model [9], as outlined in I) is described by the hamiltonian



$$H_{RVB} = -\delta t \sum_{<i,j>\sigma} (c^\dagger_{i\sigma} c_{j\sigma} + h.c.) - J \sum_{<i,j>} b^\dagger_{ij} b_{ij} \qquad (2)$$

where '$t$' and '$J$' are the nearest neighbour hopping and the superexchange integrals respectively with $J = 2t^2/U$, '$U$' being the Coulomb correlation and < ..... > denotes the nearest neighbours. The projection operators in the hopping integral are being approximated by the dopant concentration $\delta$. $b^\dagger_{ij} = \frac{1}{\sqrt{2}}(c^\dagger_{i\uparrow} c^\dagger_{j\downarrow} - c^\dagger_{i\downarrow} c^\dagger_{j\uparrow})$, is the valence bond singlet oprator and $c_{i,\sigma}(c^\dagger_{i,\sigma})$, is the usual fermion annihilation (creation) operator with spin '$\sigma$' at the site '$i$'.

The original BZA mean field (MF) theory [7] is almost identical to the BCS theory of superconductivity in its mathematical structure except for a k-dependence of the BZA mean field order parameter. This is a natural consequence of the fact that the BZA MF ground state consists of a collection of nearest neighbour singlet pairs in real space. Therefore, it has been presumed [7] that as soon as one allows for the coherent motion of the singlet pairs by doping holes into the BZA MF ground state, superconductivity will follow. However, it was argued in I that since the RVB state is a spin disorderd state which appears on suppressing the Neel ordered state, it will tend to modify the nature of the electronic states of the system. Because of the disorder, the electronic states particularly at the band edges will tend to be localized. As a result for small dopant concentration upto the critical value $\delta_o$, the motion of the singlet pairs will not be favoured and hence it can not give rise to superconductivity. On further increasing the dopant concentration ($\delta > \delta_o$) because of the charge on holes one goes over to

the correlated metallic state where the elementary excitations become reguuΩr fermions. As mentioned in the introduction besides these quasi particles, there would also be the fluctuations over the BZA MF state which can be visualised as the pair collective modes. The quanta of these modes are expected to have bosonic character. Therefore, in the correlated metallic state which is a model for the normal state of the high $T_c$ materials, the interaction of the quasi particles with the high frequency pair collective modes plays the most dominant role. Moreover its energy spectrum has a constant gap over parts of the Fermi surface, while in other regions it vanishes. The correlated metallic state as proposed here provides a microscopic basis for the local pair models [10]. Therefore, the hamiltonian for the correlated metallic state can be written in terms of the Nambu operators [11] $\hat{\psi}_k^\dagger = (c_{k\uparrow}^\dagger \;\; c_{-k\downarrow})$ and the Pauli matrices '$\hat{\sigma}$' as

$$H_{CMS} = H_e + H_I \tag{3}$$

where

$$H_e = \sum_k \hat{\psi}_k^\dagger[(\epsilon_k - \mu)\hat{\sigma}_o + \Delta_R(k)\hat{\sigma}_1]\hat{\psi}_k \tag{4}$$

and

$$H_I = \frac{1}{N}\sum_{k,q}\sum_{i=1}^{2}\gamma(k,q)\hat{\psi}_{k+q}^\dagger[\tilde{\Delta}_{iq}\hat{\sigma}_i]\hat{\psi}_k \tag{5}$$

with $\epsilon_k = -t\delta\gamma(k)$, $\gamma(k) = \sum_{\vec{\delta}} e^{i\vec{k}.\vec{\delta}}$, $\Delta_R(k) = J\Delta\gamma(k)$, being the BZA MF order parameter, $\Delta =< b_{ij} >$ and $\mu$ is the chemical potential. $\tilde{\Delta}_{iq} = -(J/2)\sum_k < \hat{\psi}_k^\dagger\hat{\sigma}_i\hat{\psi}_{k+q} >$



($i = 1, 2$), corresponds respectively to the amplitude and phase fluctuations of the BZA MF order parameter. However, the quantities which describe the magnitude of the corresponding deformations of the order parameter can be treated as dynamical variables. On quantising these bosonic variables, the interaction hamiltonian becomes

$$H_I = \frac{1}{N}\sum_{k,q}\sum_{i=1}^{2} J(k,q)\hat{\psi}_{k+q}^\dagger\hat{\sigma}_i\hat{\psi}_k(d_q^i + d_{-q}^{i\,\dagger}) \tag{6}$$

where $J(k,q) = J\gamma(k,q)$, $\tilde{\Delta}_{iq} = J(d_q^i + d_{-q}^{i\,\dagger}) = J\tilde{A}_q^i$. $d_q^i(d_{-q}^{i\,\dagger})$ being the bosonic annihilation (creation) operators for the $q^{th}$ quantum of the amplitude and the phase modes corresponding to i=1,2 respectively. Of course, the above hamiltonian describes the interaction of the high frequency bosons with the charge carriers of the system, while the free boson hamiltonian is given by

$$H_b = \sum_q\sum_{i=1}^{2}\Omega_q^i d_q^{i\,\dagger} d_q^i \tag{7}$$

where $\Omega_q^i$ is the frequency of the bosons corresponding to the collective modes. In order to make this theory for the normal state self consistent it is necessary to see how the interaction of eqn. (6) renormalises both the boson energies as well as the quasi particles of the RVB metallic state. This finally provides a proper description of the correlated metallic state. The calculation of the self energies involved in this process will require a knowledge of the pair polarisability function defined as

$$\chi^{p-p}(q,q',\omega) = \sum_{k,k'} << \hat{\psi}_{k+q}^\dagger(t)\hat{\sigma}_1\hat{\psi}_k(t); \hat{\psi}_{k'+q'}^\dagger(0)\hat{\sigma}_1\hat{\psi}_{k'}(0) >>_\omega \tag{8}$$

Furthermore, the calculation of the Raman intensities from the scattering by the charge carriers as well as the phonon self energies will also depend on the pair polarisability function in the limit of q=0 as will be discussed in a later section. Since in this paper we are mainly concerned with the calculation of Raman intensities, it suffices to obtain $\chi^{p-p}(q,\omega)$ for q=0. The expression for this has ben derived in I (see eqn. (36) of I), which is given by

$$\chi^{p-p}(0,\omega) = \sum_k \frac{(\epsilon_k - \mu)^2}{E_k^2} \tanh \frac{\beta E_k}{2} [\frac{1}{\omega - 2E_k} - \frac{1}{\omega + 2E_k}] \tag{9}$$

where

$$E_k = [(\epsilon_k - \mu)^2 + \Delta_R^2]^{1/2} \tag{10}$$

Equation (9) can be explicitly evaluated by replacing the summation over k by an integration over $(\epsilon_k - \mu) = \xi_k$ so that

$$\chi^{p-p}(0,\omega) = \frac{N(0)\Delta_R}{2} \int_1^{x_c} dx \frac{(x^2-1)^{1/2}}{x} \tanh \frac{\beta \Delta_R x}{2} [\frac{1}{\omega - 2\Delta_R x} - \frac{1}{\omega + 2\Delta_R x}] \tag{11}$$

where the upper limit of the integration is given by

$$x_c^2 = [1 + (\omega_c/\Delta_R)^2] \tag{12}$$

N(0) is the density of states at the Fermi level and $\omega_c$ an arbitrary cut-off frequency. In writing eqn. (11) the following substitutions are made.



$$\xi = \Delta_R \tan\theta \tag{13}$$

and

$$x = \sec\theta \tag{14}$$

It is obvious that eqn. (11) will allow for two different regions of $x$ namely $x^2 > 1 and < 1$. The real and imaginary parts of $\chi^{p-p}(0,\omega)$ are obtained by making $\omega$ complex so that eqn. (11) splits into the following equations depending the value of $x$:

Case I: $x^2 > 1$ in which case $(x^2-1)^{1/2}$ is real and the upper limit of the integration takes the value $+x_c$ so that

$$Im\chi^{p-p}(0,\omega) = \frac{-\pi N(0)\Delta_R}{2} \int_1^{x_c} dx \frac{(x^2-1)^{1/2}}{x} \tanh \frac{\beta \Delta_R x}{2} [\delta(\omega - 2\Delta_R x) - \delta(\omega + 2\Delta_R x)] \tag{15}$$

and

$$Re\chi^{p-p}(0,\omega) = \frac{-N(0)\Delta_R}{2} P \int_1^{x_c} dx \frac{(x^2-1)^{1/2}}{x} \tanh \frac{\beta \Delta_R x}{2} [\frac{1}{\omega + 2\Delta_R x} - \frac{1}{\omega - 2\Delta_R x}] \tag{16}$$

Case II: $x^2 < 1$ in which case $(x^2-1)^{1/2} = i(1-x^2)^{1/2}$ is imaginary and the upper limit takes the value $-x_c$ so that the expressions for the real and the imaginary parts just get interchanged as compared to those of eqns. (15) and (16). The imaginary part of

$\chi^{p-p}(0,\omega)$ in case I and the real part in case II involves delta functions in the integrands as in eqn. (15) so that the integrations can be easily carried out to give

$$Im\chi^{p-p}(0,\omega) = \frac{-\pi N(0)}{4}\frac{1}{(\omega/2\Delta_R)}[(\omega/2\Delta_R)^2 - 1]^{1/2}\tanh(\frac{\beta\omega}{4}) \qquad (17)$$

In case II the real part i.e; $Re\chi^{p-p}(0,\omega)$ will have the same expression with the square root term replaced by $[1-(\omega/2\Delta_R)^2]^{1/2}$. On the other hand, the real part in case I (eqn. (16)) and the imaginary part in case II involves principal value integrals which are rather difficult to carry out. Therefore, instead of calculating these quantities directly from their expression like eqn. (16), we take recourse to determine them by making use of the Kramers-Kronig analysis and the corresponding dispersion relations [12]. In doing so, the $\tanh(\frac{\beta\omega}{4})$ function involving the temperature, has been approximated for high and low temperatures as follows:

$$\tanh(\frac{\beta\omega}{4}) \approx \begin{cases} (\frac{\beta\omega}{4})[1 - 1/3(\frac{\beta\omega}{4})^2], & \beta\omega < 1 \\ sgn(\frac{\beta\omega}{4})[1 - 2\exp(-2\,|\,(\frac{\beta\omega}{4})\,|)], & \beta\omega > 1 \end{cases} \qquad (18)$$

With this eqn. (17) becomes

$$Im\chi^{p-p}(0,\omega) = -(\pi\frac{N(0)}{4})\frac{1}{(\omega/2\Delta_R)}\sqrt{(\omega/2\Delta_R)^2 - 1}\begin{cases} (\frac{\omega}{4T}), & \omega < 4T \\ 1, & \omega > 4T \end{cases} \qquad (19)$$



Furthermore, the symmetry properties of the $Im\chi^{p-p}(0,\omega)$ and $Re\chi^{p-p}(0,\omega)$ for $\omega \to -$ in the high and low temperature regions has been utilised to rewrite the dispersio relations in the region of only positive $\omega$. This simplifies the evaluation of the integral (16) upto the leading order terms in $(\beta\omega)$. Thus the real part of the pair polarisabilit function for the case $(\omega/2\Delta_R)^2 > 1$ is given by

$$Re\chi^{p-p}(0,\omega) = -(\frac{N(0)}{4})[2(\omega/2\Delta_R)\ln 2$$
$$+\sqrt{((\omega/2\Delta_R)^2 - 1)}\ln|(\frac{\sqrt{((\omega/2\Delta_R)^2 - 1)} - (\omega/2\Delta_R)}{\sqrt{((\omega/2\Delta_R)^2 - 1)} + (\omega/2\Delta_R)})|]\begin{cases} (\frac{2\Delta_R}{4T}), & \omega < 4T \\ \frac{1}{(\omega/2\Delta_R)}, & \omega > 4T \end{cases} \qquad (20$$

In obtaining the result of eqn. (20) the integrations in in the dispersion relations ar carried out in the region 1 to $\infty$ so that the condition $(\omega/2\Delta_R)^2 > 1$ is satisfied. Similarl for the case II corresponding to $(\omega/2\Delta_R)^2 < 1$, the real part of the pair polarisabilit function is given by

$$Re\chi^{p-p}(0,\omega) = -(\pi\frac{N(0)}{4})\frac{1}{(\omega/2\Delta_R)}\sqrt{1-(\omega/2\Delta_R)^2}\begin{cases} (\frac{\omega}{4T}), & \omega < 4T \\ 1, & \omega > 4T \end{cases} \qquad (21$$

The imaginary part which is calculated from eqn. (21) using the Kramers-Kronig relatic becomes

$$Im\chi^{p-p}(0,\omega) = (\frac{N(0)}{4})[\pi(\omega/2\Delta_R)$$

$$+\sqrt{(1-(\omega/2\Delta_R)^2)}\ln|(\frac{\sqrt{(1-(\omega/2\Delta_R)^2)}-1}{\sqrt{(1-(\omega/2\Delta_R)^2)}+1})|]\begin{cases}(\frac{2\Delta_R}{4T}), & \omega < 4T \\ \frac{1}{(\omega/2\Delta_R)}, & \omega > 4T\end{cases} \quad (22)$$

As expected eqns. (21) differs from eqns. (19) only in reversing the sign of the quantity within the square root. But there is a marked difference in the expressions of eqns. (20) and (22) both of which are obtained from a Kramers-Kronig analysis because in obtaining eqn. (22) the integrals are evaluated within the limit 0 to 1 so as to satisfy the condition $(\omega/2\Delta_R)^2 < 1$. This completes the analysis of the pair polarisability function. It can be easily seen that in the limit of $(\omega/2\Delta_R)^2 >> 1$ which amounts to vanishingly small gap in the normal state (i.e; $\Delta_R \rightarrow 0$), eqn. (19) reduces to

$$Im\chi^{p-p}(0,\omega)\,|_{\Delta_R-0} = -(\pi\frac{N(0)}{4})\begin{cases}(\frac{\omega}{4T}), & \omega < 4T \\ 1, & \omega > 4T\end{cases} \quad (23)$$

This is just the polarisability proposed by Varma and co-workers [2] in the phenomenological marginal Fermi liquid theory. The same result also follows from the measured Raman intensities [6]. Thus the correlated metallic state has the essential features of the marginal Fermi liquid theory in the high frequency region. However, there will be some essential difference in the low frequency region as given by eqn. (22).

In the correlated metallic state, the intensity of Raman scattering from the charge carriers will also pick up contributions from the particle-hole polarisability besides the



contributions coming from the particle-particle one. The particle-hole polarisability which is given by the density response function will also contribute to the phonon self energy as discussed in section 2. This polarisability function which is defined as

$$\chi^{p-h}(q,\omega) = \sum_{k,k'} << \hat{\psi}^{\dagger}_{k+q}(t)\hat{\sigma}_3\hat{\psi}_k(t); \hat{\psi}^{\dagger}_{k'-q}(0)\hat{\sigma}_3\hat{\psi}_{k'}(0) >>_{\omega} \quad (24)$$

can be evaluated in the correlated metallic state characterised by the pseudo-gap ($\Delta_R$) using the hamiltonian of eqn. (4). Again for the calculation of the Raman intensities, one needs its value only at q=0 and the contribution to $\chi^{p-h}(0,\omega)$ coming from the free electron part vanishes. However, since the ground state of the system is the RVB metal, there is a finite contribution proportional to $\Delta_R$, which can be deduced from eqn. (75) of I and is given by

$$\chi^{p-h}(0,\omega) = \sum_k \frac{\Delta_R^2}{4E_k^2}\tanh\frac{\beta E_k}{2}[\frac{1}{\omega-2E_k} - \frac{1}{\omega+2E_k}] \quad (25)$$

The real and imaginary parts of eqn. (25) can be calculated by following the procedure exactly similar to that discussed for the calculation of the particle-particle polarisability. Again splitting the frequency region into two depending on whether $(\omega/2\Delta_R)^2 > 1 or <$ 1, the results are given below.

For $(\omega/2\Delta_R)^2 > 1$

$$Im\chi^{p-h}(0,\omega) = -(\frac{\pi N(0)}{4})\frac{1}{(\omega/2\Delta_R)}\frac{1}{\sqrt{(\omega/2\Delta_R)^2-1}}\begin{cases}(\frac{\omega}{4T}), & \omega < 4T \\ 1, & \omega > 4T\end{cases} \quad (26)$$

and

$$Re\chi^{p-h}(0,\omega) = -(\frac{N(0)}{4})$$

$$[\frac{1}{\sqrt{((\omega/2\Delta_R)^2-1)}}\ln|(\frac{\sqrt{((\omega/2\Delta_R)^2-1)}-(\omega/2\Delta_R)}{\sqrt{((\omega/2\Delta_R)^2-1)}+(\omega/2\Delta_R)})|]\begin{cases}(2\Delta_R/4T), & \omega<4T\\ \frac{1}{(\omega/2\Delta_R)}, & \omega>4T\end{cases} \quad (27)$$

Similarly, for $(\omega/2\Delta_R)^2 < 1$

$$Re\chi^{p-h}(0,\omega) = -(\frac{\pi N(0)}{4})\frac{1}{(\omega/2\Delta_R)}\frac{1}{\sqrt{1-(\omega/2\Delta_R)^2}}\begin{cases}(\frac{\omega}{4T}), & \omega<4T\\ 1, & \omega>4T\end{cases} \quad (28)$$

and

$$Im\chi^{p-h}(0,\omega) = (\frac{N(0)}{4})$$

$$[\frac{1}{\sqrt{(1-(\omega/2\Delta_R)^2)}}\ln|(\frac{\sqrt{(1-(\omega/2\Delta_R)^2)}-1}{\sqrt{(1-(\omega/2\Delta_R)^2)}+1})|]\begin{cases}(2\Delta_R/4T), & \omega<4T\\ \frac{1}{(\omega/2\Delta_R)}, & \omega>4T\end{cases} \quad (29)$$

In the limit of $(\omega/2\Delta_R)^2 >> 1$ i.e: for vanishing $\Delta_R$, the imaginary part of the particle-hole polarisability vanishes as can be seen from the eqn. (25). This is in contrast to the particle-particle polarisability which gives the marginal Fermi liquid result (eqn. (23)) in this limit. Yet another general feature of the result of the finite temerature calculation presented in eqns. (19) and (22) is that the cut-off frequency does not enter explicitly



in any of these expressions. This is in contrast to the result of the zero temperatur calculation presented in I. The reason for this cut-off independence lies in the fact that i this case essentially the results are obtained purely by performing $\delta$-function integration and partly by doing a Kramers-Kronig analysis.

# 4 The Response Functions in the Superconducting State

The calculation of the Raman intensities in the superconducting state requires th evaluation of all the response functions in this state. The mechanism by which super conductivity arises in the correlated metallic state was discussed in detail in I. In wha follows, we first give a brief summary of the essential features of superconductivity i this system before presenting the results for the response functions.

As pointed out in I, superconductivity appears in the model due to the pairing c quasi particles arising out of the correlation bag mechanism. Elimination of the bosoni degrees of freedom from the interaction hamiltonian of eqn. (6) of the correlated meta result in an effective interaction between the charge carriers which is attractive and wi give rise to pairing. The result for the gap equation and the transition temperature an their dependence on the normal state gap parameter as well as the doping concentratic was discussed in I. This mechanism is expected to work in the region of rather larg dopant concentration beyond a critical value. As shown in I, in this region the transitic

temperature decreases with increasing the dopant concentration.

The polarisabilities in the superconducting state are required for the calculation of the Raman intensities at temperatures below $T_c$. These are derived in connection with the phonon response in the superconducting state and can be obtained from eqns. (83) and (84) of I. Hence the particle-particle and the particle-hole polarisabilities in the superconducting state (denoted with a subscript s) are given by

$$\chi_s^{p-p}(0,\omega) = \sum_k [\frac{3\Delta_R^2\Delta_s^2}{E_k^2 e_k} + \frac{E_k^2}{e_k} - \frac{(\Delta_R^2+\Delta_s^2)}{e_k} - \frac{\Delta_R^2 e_k}{E_k^2} + e_k + \frac{8\Delta_R\Delta_s(E_k^2-\Delta_R^2)^{\frac{1}{2}}}{E_k e_k}](\frac{\tanh(\beta e_k/2)}{\omega^2-4e_k^2}) \tag{30}$$

and

$$\chi_s^{p-h}(0,\omega) = \Delta_R^2 \sum_k [\frac{1}{e_k}(1+\frac{2\Delta_s^2}{\Delta_R^2}) - 3\frac{\Delta_s^2}{E_k^2 e_k} + \frac{e_k}{E_k^2} + \frac{8\Delta_s(E_k^2-\Delta_R^2)^{\frac{1}{2}}}{\Delta_R E_k e_k}](\frac{\tanh(\beta e_k/2)}{\omega^2-4e_k^2}) \tag{31}$$

where

$$e_k = [E_k^2 + \Delta_s^2]^{1/2} \tag{32}$$

and $\Delta_s$ is the superconducting gap parameter. The expressions within the square bracket of eqns. (30) and (31) essentially comes from the coherence factors. It is easy to check that in the limit of $\Delta_s = 0$, eqns. (30) and (31) reduce to the normal state result of eqns. (9) and (25) rspectively. In calculating the real and imaginary parts of these response functions the summation over k is replaced by an integration over $E_k$ and the density of state is taken to be a constant as done in I. As a result the signature of the normal state gap ($\Delta_R$) does not enter explicitly in the final expressions in the superconducting state, except for those entering through the coherence factors. These quantities are calculated in the low and high temperature limits following the same procedure as outlined in the normal state calculation. Thus the imaginary and the real parts of the pair polarisability function in different regions of the frequency and the temperature are as given below:

For $(\omega/2\Delta_s)^2 > 1$

$$Im\chi_s^{p-p}(0,\omega) = -(\frac{N(0)\pi}{4})\frac{1}{(\omega/2\Delta_s)(\Delta_s/\Delta_R)^2} [(\frac{3-(\omega/2\Delta_s)^2}{(\omega/2\Delta_s)^2-1}) + 2(\Delta_s/\Delta_R)^2((\omega/2\Delta_s)^2-1) - (\omega/2\Delta_s)^2]\frac{1}{\sqrt{(\omega/2\Delta_s)^2-1}} \begin{cases} (\frac{\omega}{4T}), & \omega < 4T \\ 1. & \omega > 4T \end{cases} \tag{33}$$

and

$$Re\chi_s^{p-p}(0,\omega) = -(\frac{N(0)}{4})\frac{1}{(\Delta_s/\Delta_R)^2} +[(\frac{3-(\omega/2\Delta_s)^2}{((\omega/2\Delta_s)^2-1)} + 2(\Delta_s/\Delta_R)^2((\omega/2\Delta_s)^2-1) - (\omega/2\Delta_s)^2) \frac{1}{\sqrt{((\omega/2\Delta_s)^2-1)}} \ln|(\frac{\sqrt{((\omega/2\Delta_s)^2-1)}-(\omega/2\Delta_s)}{\sqrt{((\omega/2\Delta_s)^2-1)}+(\omega/2\Delta_s)})|] \begin{cases} (2\Delta_s/4T), & \omega < 4T \\ \frac{1}{(\omega/2\Delta_s)}, & \omega > 4T \end{cases} \tag{34}$$

For $(\omega/2\Delta_s)^2 < 1$

$$Re\chi_s^{p-p}(0,\omega) = -(\frac{N(0)\pi}{4})\frac{1}{(\omega/2\Delta_s)(\Delta_s/\Delta_R)^2}$$

$$[(\frac{(\omega/2\Delta_s)^2-3}{1-(\omega/2\Delta_s)^2}) + 2(\Delta_s/\Delta_R)^2((\omega/2\Delta_s)^2-1) - (\omega/2\Delta_s)^2]\frac{1}{\sqrt{1-(\omega/2\Delta_s)^2}}\begin{cases}(\frac{\omega}{4T}), & \omega < 4T\\ 1, & \omega > 4T\end{cases} \quad (35)$$

and

$$Im\chi_s^{p-p}(0,\omega) = (\frac{N(0)}{4})\frac{1}{(\Delta_s/\Delta_R)^2}[\pi(\omega/2\Delta_s)(2(\Delta_s/\Delta_R)^2-1)$$

$$+(\frac{(\omega/2\Delta_s)^2-3}{(1-(\omega/2\Delta_s)^2)} + 2(\Delta_s/\Delta_R)^2((\omega/2\Delta_s)^2-1) - (\omega/2\Delta_s)^2)$$

$$\frac{1}{\sqrt{(1-(\omega/2\Delta_s)^2)}}\ln|(\frac{\sqrt{(1-(\omega/2\Delta_s)^2)}-1}{\sqrt{(1-(\omega/2\Delta_s)^2)}+1})|]\begin{cases}(2\Delta_s/4T), & \omega < 4T\\ \frac{1}{(\omega/2\Delta_s)}, & \omega > 4T\end{cases} \quad (36)$$

Similarly, the imaginary and the real parts of the particle-hole polarisability which follows from eqn. (31) are given in different regions as follows:

For $(\omega/2\Delta_s)^2 > 1$

$$Im\chi_s^{p-h}(0,\omega) = -(\frac{N(0)\pi}{4})\frac{1}{(\omega/2\Delta_s)(\Delta_s/\Delta_R)^2}$$

$$[(\frac{(\omega/2\Delta_s)^2-3}{(\omega/2\Delta_s)^2-1}) + 2(\Delta_s/\Delta_R)^2+1]\frac{1}{\sqrt{(\omega/2\Delta_s)^2-1}}\begin{cases}(\frac{\omega}{4T}), & \omega < 4T\\ 1, & \omega > 4T\end{cases} \quad (37)$$



and

$$Re\chi_s^{p-h}(0,\omega) = -(\frac{N(0)}{4})\frac{1}{(\Delta_s/\Delta_R)^2}$$

$$+[(\frac{(\omega/2\Delta_s)^2-3}{((\omega/2\Delta_s)^2-1)} + 2(\Delta_s/\Delta_R)^2+1)$$

$$\frac{1}{\sqrt{((\omega/2\Delta_s)^2-1)}}\ln|(\frac{\sqrt{((\omega/2\Delta_s)^2-1)}-(\omega/2\Delta_s)}{\sqrt{((\omega/2\Delta_s)^2-1)}+(\omega/2\Delta_s)})|]\begin{cases}(2\Delta_s/4T), & \omega < 4T\\ \frac{1}{(\omega/2\Delta_s)}, & \omega > 4T\end{cases} \quad (38)$$

For $(\omega/2\Delta_s)^2 < 1$

$$Re\chi_s^{p-h}(0,\omega) = -(\frac{N(0)\pi}{4})\frac{1}{(\omega/2\Delta_s)(\Delta_s/\Delta_R)^2}$$

$$[(\frac{3-(\omega/2\Delta_s)^2}{1-(\omega/2\Delta_s)^2}) + 2(\Delta_s/\Delta_R)^2+1]\frac{1}{\sqrt{1-(\omega/2\Delta_s)^2}}\begin{cases}(\frac{\omega}{4T}), & \omega < 4T\\ 1, & \omega > 4T\end{cases} \quad (39)$$

and

$$Im\chi_s^{p-h}(0,\omega) = (\frac{N(0)}{4})\frac{1}{(\Delta_s/\Delta_R)^2}$$

$$[(\frac{3-(\omega/2\Delta_s)^2}{(1-(\omega/2\Delta_s)^2)} + 2(\Delta_s/\Delta_R)^2+1)$$

$$\frac{1}{\sqrt{(1-(\omega/2\Delta_s)^2)}}\ln|(\frac{\sqrt{(1-(\omega/2\Delta_s)^2)}-1}{\sqrt{(1-(\omega/2\Delta_s)^2)}+1})|]\begin{cases}(2\Delta_s/4T), & \omega < 4T\\ \frac{1}{(\omega/2\Delta_s)}, & \omega > 4T\end{cases} \quad (40)$$

The real and imaginary parts of the polarisabilities in the normal and superconducting states contribute to the intensities of light scattered by the charge carriers and phonons in the system. In the superconducting state, the expressions for the imaginary parts of the polarisabilities which contribute to the background intensity gets modified as dictated by eqn. (33). Moreover, at low frequencies, the Raman intensity will get contributions from the imaginary parts of the polarisabilities as well as the phonon spectral density functions. Therefore, it is necessary to calculate the temperature dependence of the phonon spectral density functions which will be carried out in the next section.

# 5 Electron-Phonon Interaction and the Phonon Spectral Density Function

It was pointed out in section 2 that the Raman intensities are determined by the scattering due to charge carriers as well as the phonons. While the charge carrier scattering is proportional to the imaginary part of the polarisabilities, the phonon scattering is given by its spectral density function. The phonon response of the system requires the evaluation of its self energy which essentially depends on the nature of the ground state and of the interaction of phonons with the charge carriers in the system. Unlike the usual metals it was pointed out in I that in the correlated metallic state, there exist two different interaction mechanisms between the phonons and the charge carriers. These interactions arise because the displacements of ions from their equilibrium positions not



only modify the hopping integrals $t_{ij}$ giving rise to the usual electron-phonon interaction but also modulate the kinetic exchange integral $J_{ij}$ giving rise to a different kind of charge carrier-phonon interaction. These interaction hamiltonians ($H_{e-p}$) are derived in I and are given by

$$H_{e-p} = H^{(1)}_{e-p} + H^{(2)}_{e-p} \tag{41}$$

$$H^{(1)}_{e-p} = g \sum_{k,q,\sigma} c^{\dagger}_{k+q,\sigma} c_{k,\sigma} A_q \tag{42}$$

$$H^{(2)}_{e-p} = g' \Delta \sum_{k,q} (c^{\dagger}_{k+q\uparrow} c^{\dagger}_{-k\downarrow} + c_{-k+q\downarrow} c_{k\uparrow}) A_q \tag{43}$$

where $A_q = (b_q + b^{\dagger}_{-q})$ is the $q^{th}$ component of the phonon amplitude and the coupling constants $g$ and $g'$ are assumed to be constants independent of momenta. Note that the second interaction $H^{(2)}_{e-p}$ depends explicitly on the RVB ground state through the parameter $\Delta$, and the coupling constant $g'$ depends on the exchange integral J. It was pointed out in I that there are propagating as well as localised phonons in the system. The later arises due to the magnetic disorder created on doping the system. Because of this the localised phonons are expected to interact with the charge carriers through eqn. (43) while the interaction of the propagating phonon is given by eqn. (42). The phonon response of the system is determined by both the types of phonons and require the calculation of their propagators, which are given by

$$D^{(i)}_{q,q'}(\omega) = \delta_{-q,q'}\omega^{(i)}_q[\pi(\omega^2 - \omega^{(i)2}_q - \Pi^{(i)}(q,q',\omega))]^{-1} \tag{44}$$

where i=l,p denote the localized and the propagating modes, $\Pi^{(i)}(q,\omega)$ being their self energies. From the knowledge of the polarisations the spectral density function which is related to the imaginary part of the phonon Green's function can be evaluated as

$$S^i(0,\omega) = -2Im D^i_q(\omega + i\eta^i)\,|_{\eta=0} \tag{45}$$

$$= -\frac{2\omega^i(2\omega\eta^i + Im\Pi^i(0,\omega))}{\pi([\omega^2 - \omega^{i2} - \eta^{i2} - Re\Pi^i(0,\omega)]^2 + [2\omega\eta^i + Im\Pi^i(0,\omega)]^2)} \tag{46}$$

In writing eqn. (46) an appropriate width ($\eta^i$) is given to the bare phonons by replacing $\omega \rightarrow (\omega + i\eta^i)$ which is independent of temperature. Besides, the interaction of the phonons with the charge carriers provides temperature dependent shift and width which are given by the real and imaginary parts of the respective polarisations. These shift and width of the frequency of the phonons with q=0, are the observable quantities in the Raman measurements. In I these self energies are evaluated at zero temperature for the normal and the superconducting state. As can be seen from eqns. (47) and (48) the self energies of the localised and the propagating phonons are proportional to the particle-particle and the particle-hole polarisabilities and are given by

$$\Pi^{(i)}(0,\omega) = \begin{cases} 2\pi\tilde{g}_l\Omega_o^2\tilde{\chi}^{p-p}(0,\omega), & i = l \\ 2\pi\tilde{g}_p\omega_o^2\tilde{\chi}^{p-h}(0,\omega), & i = p \end{cases} \tag{47}$$



where the dimensionless coupling constants $\tilde{g}_l = ((g'\Delta)^2N(0)/\Omega_o)$ and $\tilde{g}_p = (g^2N(0)/\omega$
, $\Omega_o$ and $\omega_o$ being the frequencies of the localised and the propagating phonons and

$$\tilde{\chi}(0,\omega) = \chi(0,\omega)/(N(0)\pi/4) \tag{48}$$

The pair and particle-hole polarisabilities in the normal and the superconducting sta have been explicitly evaluated at finite temperatures in section 3 and 4. Hence the together with eqns. (47) and (48) when substituted into eqn.(46) give the phon spectral density function.

## 6 Results and Discussion

The stage is now set to calculate the temperature dependence of the Raman intensit using eqns. (1) and (46-48). It is evident from eqn. (1) that the intensities p up contributions coming from (i) the scattering by the charge carriers given by t imaginary parts of the polarisabilities and (ii) the scattering by the phonons given the phonon spectral density functions. In contrast, in paper I only the later cntribut was calculated at zero temperature and a constant intensity background was ad by hand. The number of phonons observed in the Raman spectrum varies from cuprate to another, in particular in the case of the 123 systems there appears th phonons as mentioned in the introduction. Since our aim is not to make a quantita comparision with the observed spectrum but only to explain its qualitative features, confine ourselves to the calculation of only two spectral density functions one for eit

category namely the propagating and the localised phonons as was done also in I. It can be seen from the eqns. (19-22), (26-29) and (33-40) for the polarisabilities in the normal and superconducting states as well as the eqn. (46) for the phonon spectral density functions that the finite temperature results unlike the zero temperature ones are independent of any cut-off frequency. This is a remarkable improvement over the zero temperature calculation of I.

It was pointed out in I that the model for the correlated metallic state and that for superconductivity are valid only in the region of large dopant concentrations. However, in principle the results for the polarisabilities presented in eqns.(8) and (24) of this paper are valid in the entire dopant concentration region starting from that of the low corresponding to the insulating RVB state to the high concentrations where the ground state is the correlated metallic state. The only way we distinguish between them is by noting that in the insulating state the RVB gap exists all over the Fermi surface, where as in the correlated metallic state it vanishes over large regions of the Fermi surface, existing only in small portions. This has been incorporated into our calculation by rewriting the k-sums in the polarisabilities as having two different contributions in the normal state as

$$\sum \longrightarrow \sum_{k\epsilon\Delta_R\neq 0} + \sum_{k\epsilon\Delta_R=0} \tag{49}$$

which is similar to the approximation introduced by Bilbro and McMillan [15] for the case of charge density wave superconductors. Eqn. (49) is equivalent to breaking up the



density of states at the Fermi level into two parts such that

$$N(0) = N_1(0) + N_2(0) \tag{50}$$

Where $N_1(0)$ is the free electron density of states at the Fermi level associated with the region where the RVB gap $\Delta_R \neq 0$ and $N_2(0)$ is that for the region where the RVB gap tends to zero. So that the polarisabilities will pick up contributions coming from $(\omega/2\Delta_R)^2 < 1$ with a weight factor $(N_1(0)/N(0))$ and another contributions coming from $(\omega/2\Delta_R)^2 >> 1$ with a weight factor $(N_2(0)/N(0))$. Note that the second contribution is actually the polarisability of the marginal Fermi liquid state as given by eqn. (23) for the pair polarisabilty function. In this scheme if $N_1(0) >> N_2(0)$ it will correspond to the low dopant or the RVB insulator regime and if $N_2(0) >> N_1(0)$ it will correspond to the correlated metallic state. Since the constant intensity background in the Raman spectrum arises from the polarisabilities, in principle the present model predicts the existance of the background intensity starting from the insulating to the Fermi liquid like metallic state as has actually been observed both in the 214 [6] and the 123 [5] systems. However, in the present calculation our main concern is the behaviour of the Raman spectrum in the correlated metallic state, therefore in all the numerical calculations we take $N_2(0) > N_1(0)$ ($[N_2(0)/N(0)] = 0.7$ and $[N_1(0)/N(0)] = 0.3$). Moreover in the calculation of the polarisabilities several constraints (such as $(\omega/2\Delta_R)^2 > 1 and < 1$ and also $(\omega/4T) > 1 and < 1$) are introduced, which requires a more careful analysis [16], in keeping track of the regions of validity of these constraints.

The phonon-Raman scattering measurements are mostly confined to the analysis of the temperature dependent shift and width of the phonons. These quantities are expected to show different behaviour depending on whether the phonon lies above or below the superconducting gap. An analysis based on the strong coupling theory by Zeyher and Zwicknagl [17] predicts that the phonon with frequency higher than the superconducting gap will undergo softening and broadening on lowering the temperature below the superconducting transition temperature ($T_c$). On the otherhand, a phonon with frequency less than the superconducting gap will sharpen on going below ($T_c$). This is so simply because below ($T_c$) the density of states within the gap vanishes and hence the width arising from the electron-phonon interaction is expected to vanish. Similarly on opening the superconducting gap the density of states just above the gap increase which will result in the broadening of the phonon lying above the gap. In contrast to the strong coupling theory, the weak coupling analysis always predicts the hardening of the phonon frequency. The predictions of these theories are based on the fact that the phonon interacts with the charge carriers through the normal electron-phonon interaction, so that the phonon self energies involve only the electron-hole polarisability. In contrast, the present theory has two different charge carrier-phonon couplings which involve the electron-hole as well as the pair polarisabilities for the self energies. Hence the temperature dependence of the phonons in this case are expeted to be quite different even within a weak coupling theory. Therefore, an analysis of the phonon shift and width in the present model is going to be important from the point of view of testing



the model.

In all the numerical results the Raman intensities in arbitrary units are plotte against the reduced frequency ($\omega/\omega_o$), $\omega_o$ being the frequency of the propagating phonor Furthermore, the calculation involves several dimensionless parameters such as the rati of the frequencies of the propagating and the localised phonons ($\omega_o/\Omega_o$), the ratio of th phonon frequency to the normal state gap parameter ($\omega_o/2\Delta_R$), the width of the bar phonons ($\eta^l/\Omega_o$) and ($\eta^p/\omega_o$) as well as the coupling constants for the phonon charg carrier interaction $\tilde{g}_l$ and $\tilde{g}_p$, besides the ratio of the phonon frequencies to the tem perature ($\omega_o/4T$). On going over to the superconducting state one must add two mor parameters to the list corresponding to the superconducting gap parameter ($\omega_o/2\Delta_s$ and the ratio between the superconducting to the normal state gap parameters ($\Delta_s/\Delta_R$ In all the calculations in the superconducting state it is usually assumed that the super conductivity appears over the normal state gap, so that $\Delta_s << \Delta_R$. However, in all th calculations the values of the three of these parameters namely, the bare phonon width ($\eta_l/\Omega_o$) and ($\eta_p/\omega_o$) as well as the ratio between both the phonon frequencies is kep fixed. The later is so chosen that the frequency of the localised phonon is twice that c the propagating phonon ($i.e; (\omega_o/\Omega_o) = 0.5$). The results pertaining to the variation c the rest of the parameters are presented in Figs. (1-14).

## 6.1 Raman Intensity in the Correlated Metallic State

The variation of the Raman intensity with the variation of different parameters such as temperature ($\omega_o/4T$), the normal state gap parameter ($\omega_o/2\Delta_R$) and both the coupling constants $\tilde{g}_l$ and $\tilde{g}_p$ are plotted in figs. 1-7. In all these plots, the coupling constant, frequency and the width of the localised phonon are assumed to be larger than those of the propagating phonon. Moreover, the frequencies of both the phonons are taken to be less than the normal state gap parameter, as noted in every figure. Since the intensities are plotted as a function of the reduced frequency, the peaks corresponding to propagating and localised phonons are expected to appear around $(\omega/\omega_o) = 1 and 2$ respectively. As mentioned earlier, the intensities in the normal state are obtained by substituting eqns. (19-22), (26-29) and (46) in eqn. (1). In looking at the temperature dependence of the spectra, the high and the low temperature behaviour are plotted separately. In fact, in the low temperature region, the entire spectrum becomes temperature independent as can be seen from the above equations.

Fig. 1 shows the temperature dependence of the Raman intensity. The decreasing of the parameter ($\omega_o/4T$) from 0.4 to 0.3 is equivalent to increasing temperature. Therefore, with decreasing temperature the intensities of both the phonons decrease while their frequencies soften by a small amount. Moreover, both the phonons broaden with decreasing temperature, this effect being more noticeable for the localised phonon. Besides, an increase in the intensity as the frequency tends to zero as well as a constant intensity background at high frequencies are features associated with the scattering by



the charge carriers.

Figs. 2 and 3 shows the variation of the Raman intensity with the normal state gap parameter ($\omega_o/2\Delta_R$), at high ($\omega > 4T$) and low ($\omega < 4T$) temperatures respectively. As the parameter increases from 0.25 to 0.35 for $\omega < 4T$ and from 0.25 to 0.75 for $\omega > 4T$, the normal state gap increases. This feature can also be correlated to the variation of the dopant concentration in the sense that a decrease in $\Delta_R$ amounts to an increase in the dopant concentration. As can be seen from fig. 2 for $\omega < 4T$ with increasing $\Delta_R$, the intensities of both the phonons decrease. But the localised phonon softens while there is no change in the frequency of the propagating one. Associated with these effects is a little broadening of both the phonons. For $\omega > 4T$, as can be seen from fig. 3, the constant intensity background extends upto very high frequency and decreases slightly with decreasing $\Delta_R$. In this plot, a discontinuity appears around $(\omega/\omega_o) = 4$ for the $(\omega/2\Delta_R) = 0.2$ which moves to lower frequencies with decreasing $\Delta_R$. This is a signature of the normal state gap. The intensity of the propagating mode decreases with increasing $\Delta_R$ and the peak broadens, while its frequency softens. Similar effects can also be seen in the case of the localised mode.

Figs.4-7 depicts the variation of the intensities on varying the strength of the charge carrier-phonon interaction. Only one of the coupling constant is varied at a time and the results for high and low temperatures are depicted separately. One general feature of all the curves is that with increasing coupling constant the width of the corresponding phonon increases and the intensity decreases to the extent that beyond a certain value of

the coupling constant the phonon vanishes. Furthermore, with increasing the strength of the interaction phonon softens at high temperatures (figs. 4 and 6 ) while it hardens at low temperatures (figs. 5 and 7). It should be mentioned that the Raman intensities of the phonons are very sensitive to the values of the coupling constants. In the case of localised phonon however there is a marked increase in the background intensity at low frequencies with decreasing coupling constants.

## 6.2 Raman Intensities in the Superconducting State

Figures 8-14 depict the Raman intensities in the superconducting state corresponding to the variation of the temperature, the superconducting gap parameter and the coupling constants for the localised and the propagating phonons as in the earlier case of the normal state. The only difference being the variation of the superconducting gap ($\Delta_s$) in the present case compared to that of the normal state gap ($\Delta_R$) in the earlier discussion. Since $\Delta_s$ is always smaller than $\Delta_R$, the characteristic temperature demarketing the high and low temperature behaviour is much smaller. Hence the discontinuity corresponding to the superconducting gap always appear in both the high and the low temperature plots. Besides, the choice of the parameters is such that the frequencies of the propagating and the localised phonons are below and above the superconducting gap. A general feature in all these plots is that in the superconducting state, the constant intensity background is much smaller than in the correlated metallic state.

Figure 8 shows that with decreasing temperature the frequency of the localised



phonon hardens while its width increases and intensity decreases. The later conclusions regarding the width and intensity hold good for the propagating phonon as well. But the frequency of the propagating phonon softens with decreasing temperature.

With decreasing the superconducting gap the intensity of the localised phonon increases and its frequency softens while the width decreases for the high temperature case as can be seen from fig. 9. The same conclusions also hold good for the propagating phonon at a much smaller scale. In the low temperature case as can be seen from fig. 10 the local mode softens drastically with decreasing $\Delta_s$. Its intensity increases and width decreases slightly. For the propagating phonon there is just an increase in intensity with decreasing $\Delta_s$.

The variation of the phonon intensity, frequency and width with varying coupling constants are depicted in figs. 11-14. With increasing coupling constant the intensity of the localised mode decreases while its frequency and width increases in both high and low temperature limits as can be seen from figs. 11 and 12. The behaviour for the propagating phonon as depicted in figs. 13-14 shows a softening with increasing coupling constant. This behaviour is in contrast with that of the normal state where both the propagating and the localised phonons soften at high temperature while they harden in the low temperature limit with increasing coupling constants.

The behaviour of the calculated Raman spectra discussed above shows qualitative similarity with detailed measurements carried out recently. As pointed out in the introduction, these measurements have focussed their attention on mainly two differen

aspects namely (i) the variation of the continuum intensity with varying dopant concentration [5, 6, 18] and (ii) the dopant concentration and temperature dependence of the shift and width of various phonons [4]. One of the important results from the former measurements on the continuum scattering seen in both $La_{2-x}Sr_xCuO_4$ [6] as well as in $YBa_2Cu_3O_{7-y}$ [5, 18] is that a background intensity has been observed in the ranges of the dopant concentrations corresponding to the metallic, superconducting and even in the insulating state. This led to the conclusion that the continuum intensity in the metallic and the insulating states may be arising from the free and localised (pairs) charge carriers respectively. In the present calculation, it is shown how the continuum intensity arises microscopically within the model of the correlated metallic state. Besides, at low dopant concentration the model being that of an RVB insulator, it contains local pairs, the scattering from which can give rise to a constant intensity background. Thus the predictions of the theory is in agreement with the experimental results. The variation of the intensity on going from metallic to superconducting state is also in qualitative agreement with the Raman data.

The second aspect namely the detailed observation of the temperature dependent shift and width of the phonons in the 123 compound having different oxygen contents [4] also provides much useful information regarding the metallic and the superconducting states of the system. A detailed discussion of the experimental situation is presented in the introduction. In particular, the observation of the softening of the $500cm^{-1}$ phonon below $\sim 80K$ in the deoxygeneted sample with a $T_c$ of 60 K is very significant. On



comparing with the behaviour of the $340cm^{-1}$ phonon which softens on going below the superconducting transition temperature of 93 K in samples with the oxygen content of 6.93 or more; one can conclude that there is a gap in the normal state. This observation fits in very nicely with our model of the correlated metallic state, where there exists a gap ($\Delta_R$). In fact, it is clearly shown in figs.1-7 that there is a shift in frequency and change in width of both the categories of phonons in the normal state. The shift could correspond to a softening or hardening under various conditions while the change in width always corresponds to a broadening. The shift and change in width of of the phonons persist in the superconducting state as well. However, in different regions of temperature this may or may not agree with the observed behaviour in the normal state. Furthermore, from the observed assymmetry of the line shapes of the different phonons one can draw inferences about the variation of the strength of interction of the phonons with the charge carriers in the system. The experimental results show that the $340cm^{-1}$ phonon becomes more symmetric on going from oxygeneted to the deoxygeneted samples indicating that its coupling with charge carriers decreases on deoxygenetion. On the otherhand, the $500cm^{-1}$ phonon becomes more assymmetric on going to deoxygeneted samples. This indicates that the coupling of the $500cm^{-1}$ mode with the charge carriers increases in the deoxygeneted samples, while the reverse is true for the $340cm^{-1}$ phonon. Comparision of the theory with the experimental facts is possible if we assign the local phonon to be the $500cm^{-1}$ mode and the propagating phonon to be the $340cm^{-1}$ mode. Thus the features of the experimental Raman spectrum can be qualitatively understood.

# 7 Conclusion

The Raman intensities are calculated from first principles for the model of the correlated metallic state and the superconducting state arising due to the bag mechanism as proposed in I. These models for the normal and the superconducting states are expected to represent the features of the cuprate superconductors in the large dopant concentration range. The calculation sucessfully explains the constant intensity background arising due to the scattering by the charge carriers in the system. This continuum scattering is proportional to the imaginary part of the polarisabilities. In the limit of vanishing of the normal state gap, the imaginary part of the pair polarisability function reproduces the marginal Fermi liquid behaviour. The phonon response functions are calculated using these polarisabilities. The calculated shift in frequency and the change in linewidth of the phonons show qualitative agreement with the experimental results.

There have been other attempts to calculate the continuum scattering by charge carriers [19]. In these calculations only the contribution of the electron-hole polarisability is taken into account, since the normal state is assumed to be that of a Fermi liquid. The imaginary part of the electron-hole polarisability is calculated for finite but small momentum transfers, by providing a phenomenological width to the plasmon peak as dictated by the marginal Fermi liquid theory. As a result, the plasmon peak broadens to resemble the continuum scattering, however beyond a certain cut-off value it decreases and goes to zero. The cut-off in this procedure enters through the width of the phenomenological marginal Fermi liquid theory. The essential difference between this



calculation and that of ours lies in the fact that the normal state in our theory is no a Fermi liquid like metal but a correlated metal which has a built in gap due to qua particle pairs. Therefore the Raman scattering picks up contributions due to the pa fluctuation effects which is represented by the imaginary part of the pair polarisabilit Thus the scattering cross section acquires a finite value even at zero momentum transfe which will be strictly zero in the other theory [19].

**Acknowledgements:** The authors would like to thank Prof. J. C. Irwin for sending the preprint of their results of measurements prior to publication. One of us (S.N.B would also like to acknowledge useful discussions with Dr. M.R.Press.

## References


[1] S. L. Cooper and M. V. Klein, Comments Cond. Mat. Phys. **15**, (1990), 99 and C. Thomsen and M. Cardona in "The Physical Properties of High Temperature Superconductors" Vol.I, Ed. by D. M. Ginsberg, (World Scientific Press, Singapore, 1989), Ch. VIII.

[2] C. M. Varma, P. B. Littlewood, S. Schmitt-Rink, E. Abrahams and A. E. Ruckenstein, Phys. Rev. Lett. **63**, (1989), 1996 and C. M. Varma, Int. Journal of Mod. Phys. B **3**, (1989), 2083.

[3] Debanand Sa and S. N. Behera, Physica C **203**, (1992), 347.

[4] E. Altendorf, J. C. Irwin, R. Liang and W. N. Hardy, Solid State Comm. **80**, (1991), 627; E. Altendorf, X. K. Chen, J. C. Irwin, R. Liang and W. N. Hardy, (1992) Simon Fraser University Preprint and References therein.

[5] A. A. Maksimov, A. V. Puchkov, I.I. Tartakovskii, D. Reznik, M. V. Klein, W. C. Lee and D. M. Ginsberg, JETP Lett. **56**, (1992), 570.

[6] S. Sugai, Solid State Comm. **76**, (1990), 365.

[7] B. Baskaran, Z. Zou and P. W. Anderson, Solid State Comm. **63**, (1987), 973.

[8] J. R. Schrieffer, X. G. Wen and S. C. Zhang, Phys. Rev. B **39**, (1991), 11663.

[9] J. Hubbard, Proc. Roy. Soc. London A **276**, (1963), 238.





[10] L. N. Bulaevskii, A. A. Sobyanin and D. I. Khomskii, Sov. Phys. JETP **60**, (1984), 856; J. Ranninger and S. Robaszkiewicz, Physica B **135**, (1985), 468; S. Robaszkiewicz, R. Micnas and J. Ranninger, Phys. Rev. B **36**, (1987), 180; G. M. Eliasberg, JETP Lett. **46**, Supplement, (1987), S81; I. O. Kulik, Int. Journal of Mod. Phys. B **2**, (1988), 851; D. I. Khomskii and A. K. Zvezdin, Solid State Comm. **66**, (1988), 66; K. P. Sinha and M. Singh, J. Phys. C, S. S. P. **21**, (1988), L231; D. I. Khomskii, Phys. Lett. A **138**, (1989), 435; R. Friedberg and T. D. Lee, Phys. Lett. A **138**, (1989), 423; Y. Bar Yam, Phys, Rev. B **43**, (1991), 359, ibid. **43**, (1991), 2601; B. R. Alascio, R. Allub, C. R. Proetto and C. I. Ventura, Solid State Comm. **77**, (1991), 949; C. I. Ventura, B. R. Alascio and R. Allub, (1991), Bariloche preprint.

[11] I. O. Kulik, O. Entin-Wohlman and R. Orbach, J. Low Temp. Phys. **34**,(1981), 591.

[12] See G. Arfken, "Mathematical Methods for Physicists", (Academic Press, 1985) P. 421.

[13] See I. S. Gradshteyn and I. M. Ryzhik, "Table of Integrals, Series, and Products" (Academic Press, 1965).

[14] M. V. Klein in "Light Scattering in Solids" Vol. III, Ch. 5 Ed. by M. Cardona and G. Guntherdort (Springer Verlag, Berlin 1982).

[15] G. Bilbro and W. L. McMillan, Phys. Rev. B **14**, (1976), 1887.

[16] Debanand Sa and S. N. Behera, (1993), To be communicated.

[17] R. Zeyher and G. Zwicknagl, Z. Phys. B 78, (1990), 175.

[18] D. Reznik, S. L. Cooper, M. V. Klein, W. C. Lee, D. M. Gingberg and S. W. Cheong in "Electronic Properties of High $T_c$ Superconductors", Ed. H.Kuzmany M. Mehring and J. Fink, Springer series in Solid State Sciences 113, (Springer Verlag, Berlin 1993) p. 215.

[19] M. R. Press and S. S. Jha, Physica C 201, (1992), 21 and References therein.



## FIGURE CAPTIONS:

Figure 1: Raman intensity in the normal state as a function of the reduced frequency due to the variation in $\omega_o/4T$ for the case where the frequency is less than the temperature ($\omega < 4T$).

Figure 2: Raman intensity in the normal state as a function of the reduced frequency due to the variation in $\omega_o/2\Delta_R$ for the case where the frequency is less than the temperature ($\omega < 4T$).

Figure 3: Raman intensity in the normal state as a function of the reduced frequency due to the variation in $\omega_o/2\Delta_R$ for the case where the frequency is greater than the temperature ($\omega > 4T$).

Figure 4: Raman intensity in the normal state as a function of the reduced frequency due to the variation in $\tilde{g}_l$ for the case where the frequency is less than the temperature ($\omega < 4T$).

Figure 5: Raman intensity in the normal state as a function of the reduced frequency due to the variation in $\tilde{g}_l$ for the case where the frequency is greater than the temperature ($\omega > 4T$).

Figure 6: Raman intensity in the normal state as a function of the reduced frequency due to the variation in $\tilde{g}_p$ for the case where the frequency is less than the temperature ($\omega < 4T$).

Figure 7: Raman intensity in the normal state as a function of the reduced frequency due to the variation in $\tilde{g}_p$ for the case where the frequency is greater than the temperature ($\omega > 4T$).

Figure 8: Raman intensity in the superconducting state as a function of the reduced frequency due to the variation in $\omega_o/4T$ for the case where the frequency is less than the temperature ($\omega < 4T$).

Figure 9: Raman intensity in the superconducting state as a function of the reduced frequency due to the variation in $\omega_o/2\Delta$, for the case where the frequency is less than the temperature ($\omega < 4T$).

Figure 10: Raman intensity in the superconducting state as a function of the reduced frequency due to the variation in $\omega_o/2\Delta$, for the case where the frequency is greater than the temperature ($\omega > 4T$).

Figure 11: Raman intensity in the superconducting state as a function of the reduced frequency due to the variation in $\tilde{g}_l$ for the case where the frequency is less than the temperature ($\omega < 4T$).

Figure 12: Raman intensity in the superconducting state as a function of the reduced frequency due to the variation in $\tilde{g}_l$ for the case where the frequency is greater than the temperature ($\omega > 4T$).



Figure 13: Raman intensity in the superconducting state as a function of the reduced frequency due to the variation in $\tilde{g}_p$ for the case where the frequency is less than the temperature ($\omega < 4T$).

Figure 14: Raman intensity in the superconducting state as a function of the reduced frequency due to the variation in $\tilde{g}_p$ for the case where the frequency is greater than the temperature ($\omega > 4T$).

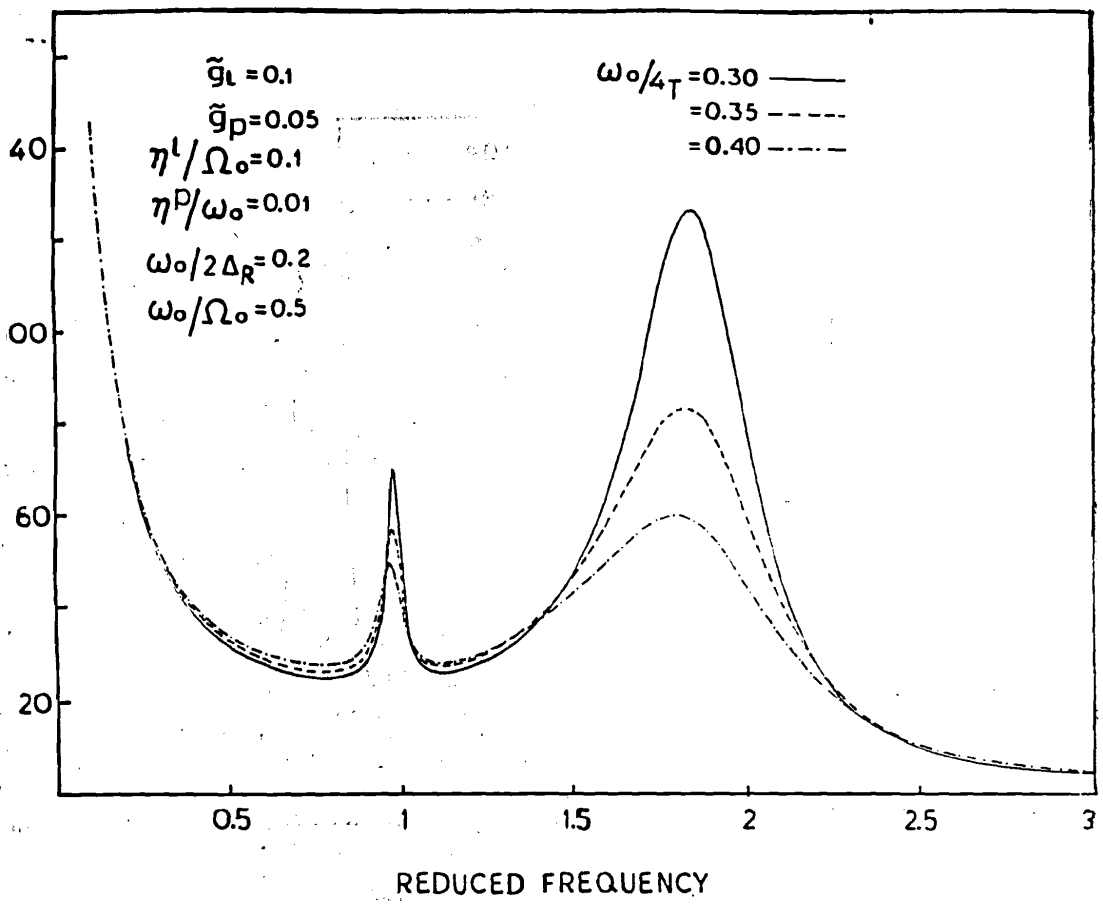
$\tilde{g}_l = 0.1$
$\tilde{g}_p = 0.05$
$\eta^l/\Omega_o = 0.1$
$\eta^p/\omega_o = 0.01$
$\omega_o/2\Delta_R = 0.2$
$\omega_o/\Omega_o = 0.5$
$\omega_o/4_T = 0.30$
$= 0.35$
$= 0.40$
40
00
60
20
0.5
1
1.5
2
2.5
3
REDUCED FREQUENCY

Fig.1

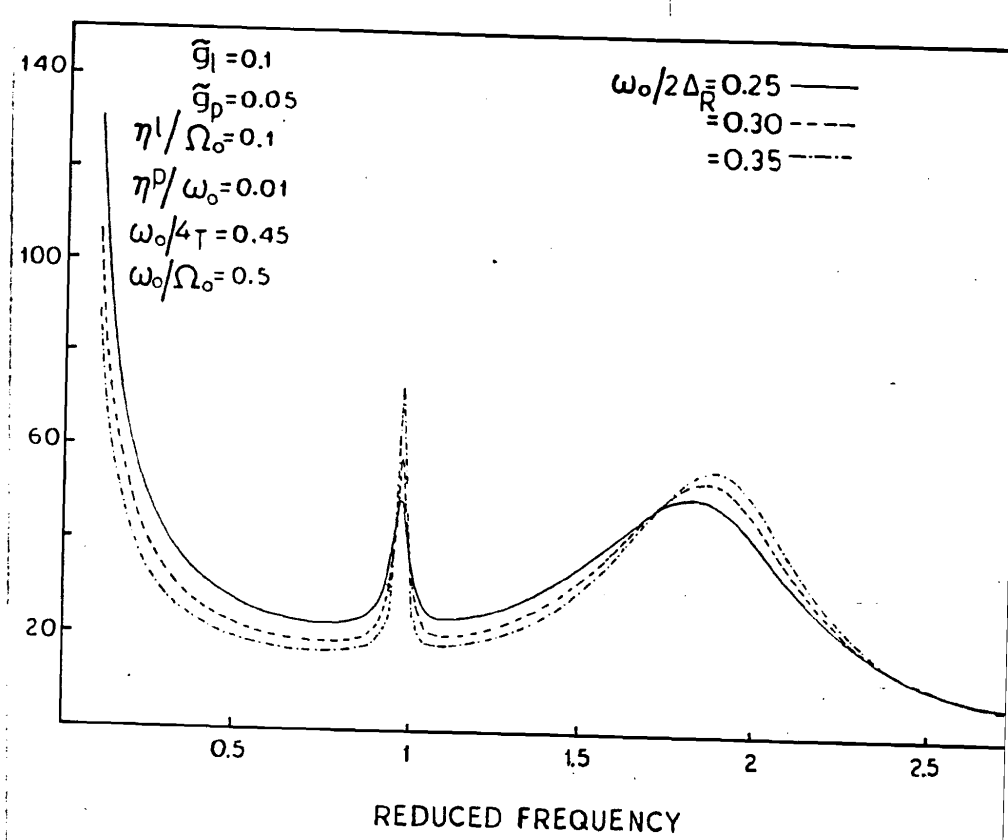
$\tilde{g}_l = 0.1$
$\tilde{g}_p = 0.05$
$\eta^l/\Omega_o = 0.1$
$\eta^p/\omega_o = 0.01$
$\omega_o/4_T = 0.45$
$\omega_o/\Omega_o = 0.5$
$\omega_o/2\Delta_R = 0.25$
$= 0.30$
$= 0.35$
140
100
60
20
0.5
1
1.5
2
2.5
REDUCED FREQUENCY

Fig.2

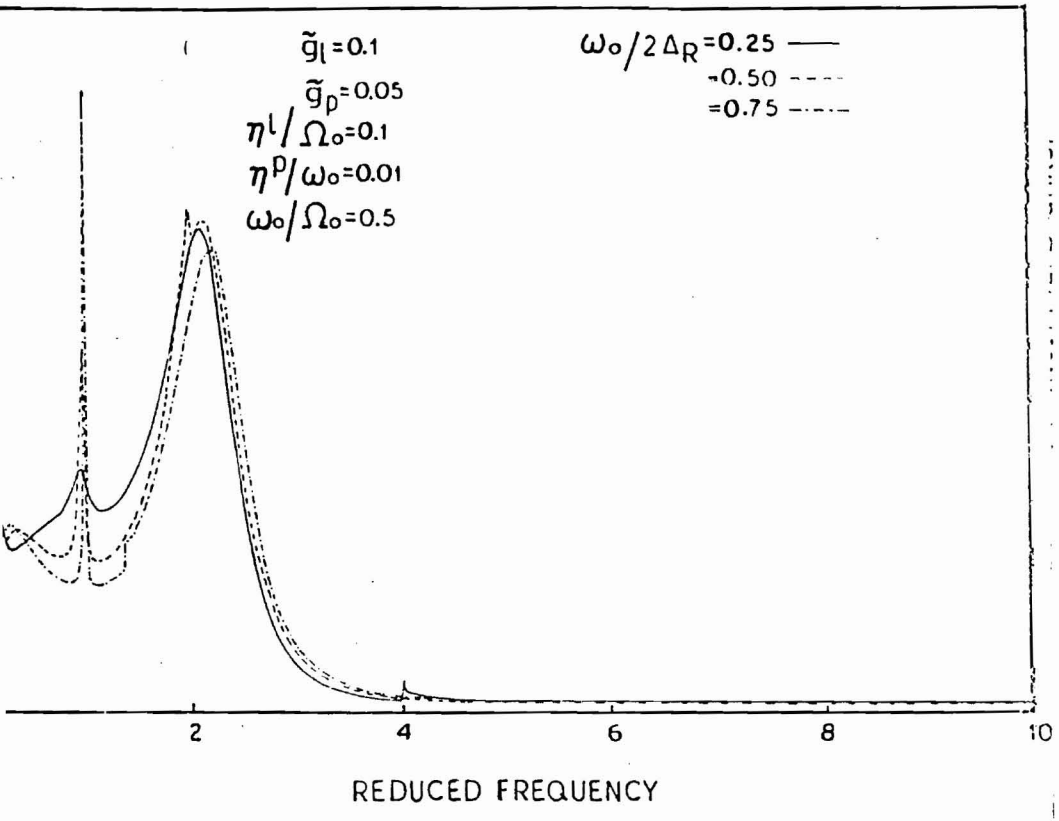
$\tilde{g}_l = 0.1$
$\tilde{g}_p = 0.05$
$\eta^l/\Omega_o = 0.1$
$\eta^p/\omega_o = 0.01$
$\omega_o/\Omega_o = 0.5$
$\omega_o/2\Delta_R = 0.25$
$= 0.50$
$= 0.75$
2
4
6
8
10
REDUCED FREQUENCY

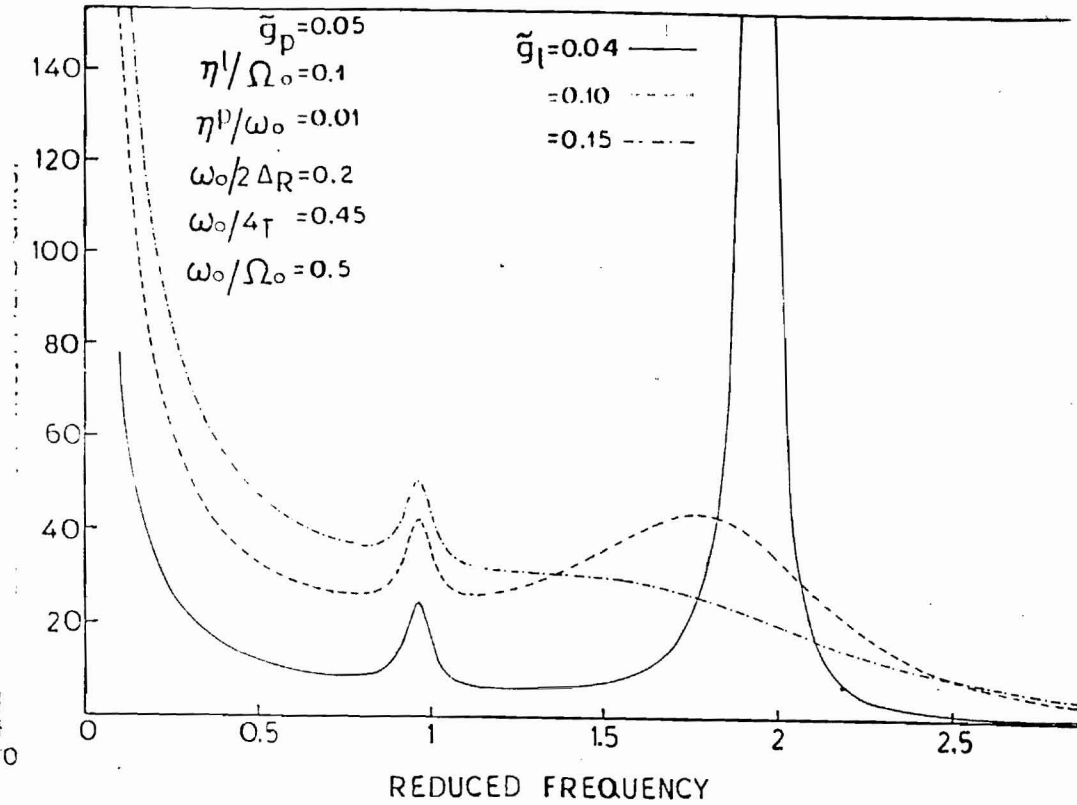
$\tilde{g}_p = 0.05$
$\eta^l/\Omega_o = 0.1$
$\eta^p/\omega_o = 0.01$
$\omega_o/2\Delta_R = 0.2$
$\omega_o/4_T = 0.45$
$\omega_o/\Omega_o = 0.5$
$\tilde{g}_l = 0.04$
$= 0.10$
$= 0.15$
140
120
100
80
60
40
20
0
0.5
1
1.5
2
2.5
REDUCED FREQUENCY

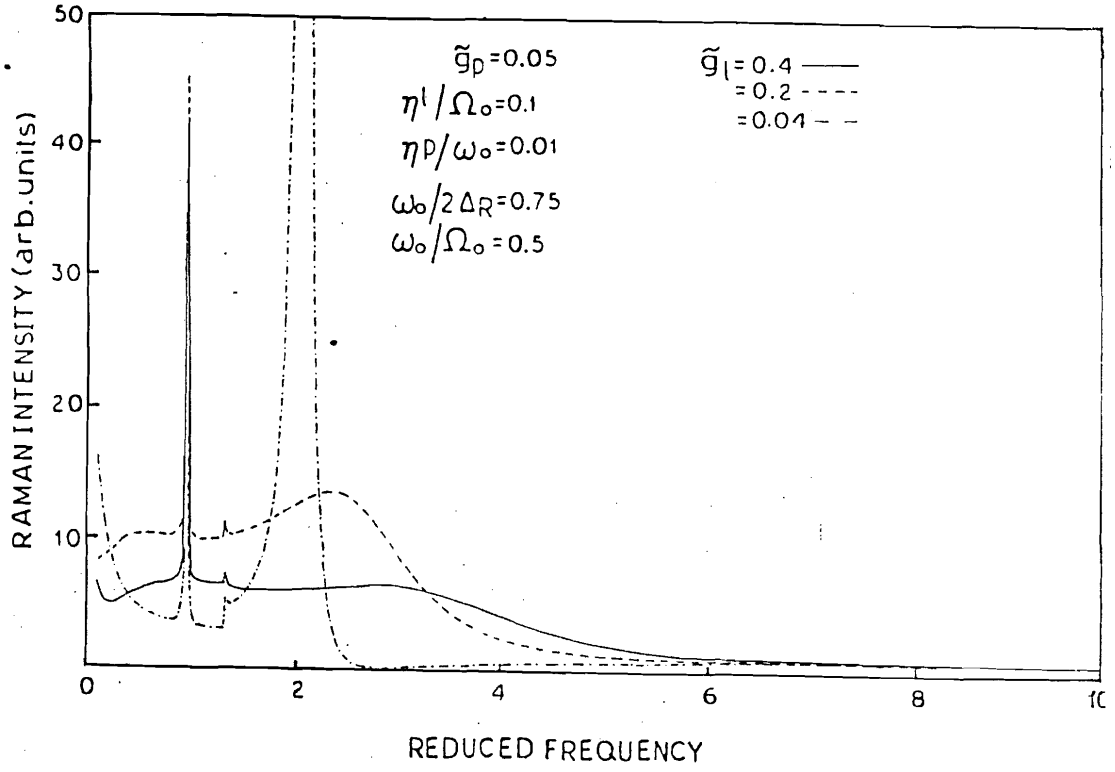
$\tilde{g}_p = 0.05$
$\eta^l / \Omega_o = 0.1$
$\eta^p / \omega_o = 0.01$
$\omega_o / 2\Delta_R = 0.75$
$\omega_o / \Omega_o = 0.5$
$\tilde{g}_l = 0.4$
$= 0.2$
$= 0.04$
RAMAN INTENSITY (arb.units)
REDUCED FREQUENCY
0
2
4
6
8
10
10
20
30
40
50

Fig 5

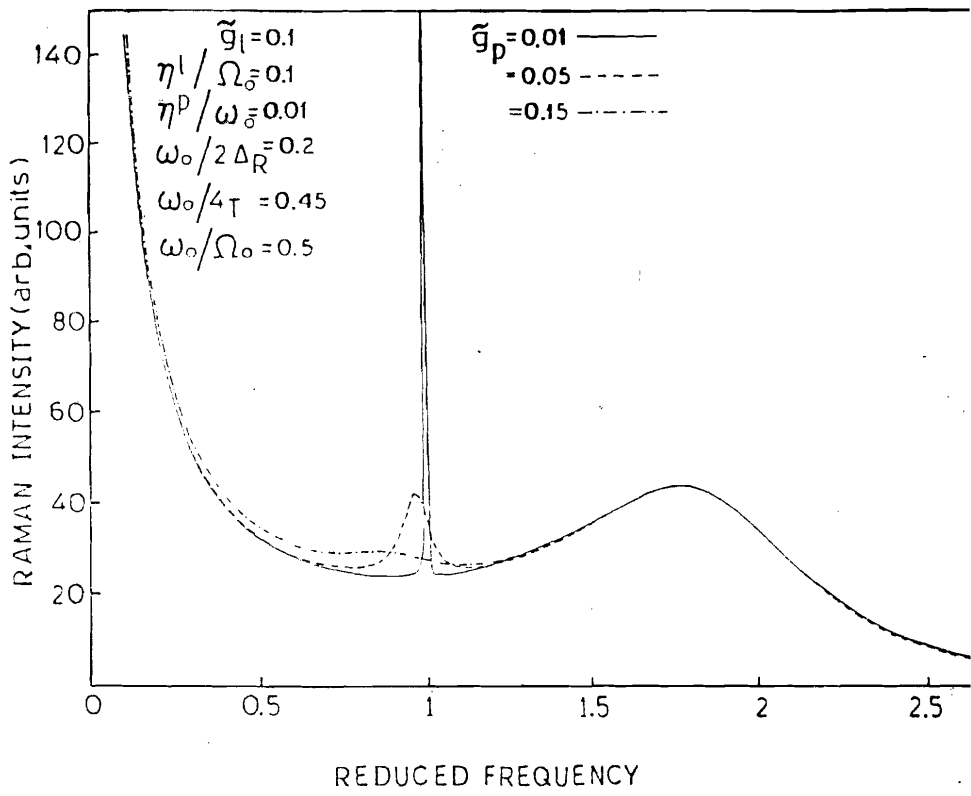
$\tilde{g}_l = 0.1$
$\eta^l / \Omega_o = 0.1$
$\eta^p / \omega_o = 0.01$
$\omega_o / 2\Delta_R = 0.2$
$\omega_o / 4_T = 0.45$
$\omega_o / \Omega_o = 0.5$
$\tilde{g}_p = 0.01$
$= 0.05$
$= 0.15$
RAMAN INTENSITY (arb.units)
REDUCED FREQUENCY
0
0.5
1
1.5
2
2.5
20
40
60
80
100
120
140

Fig.6

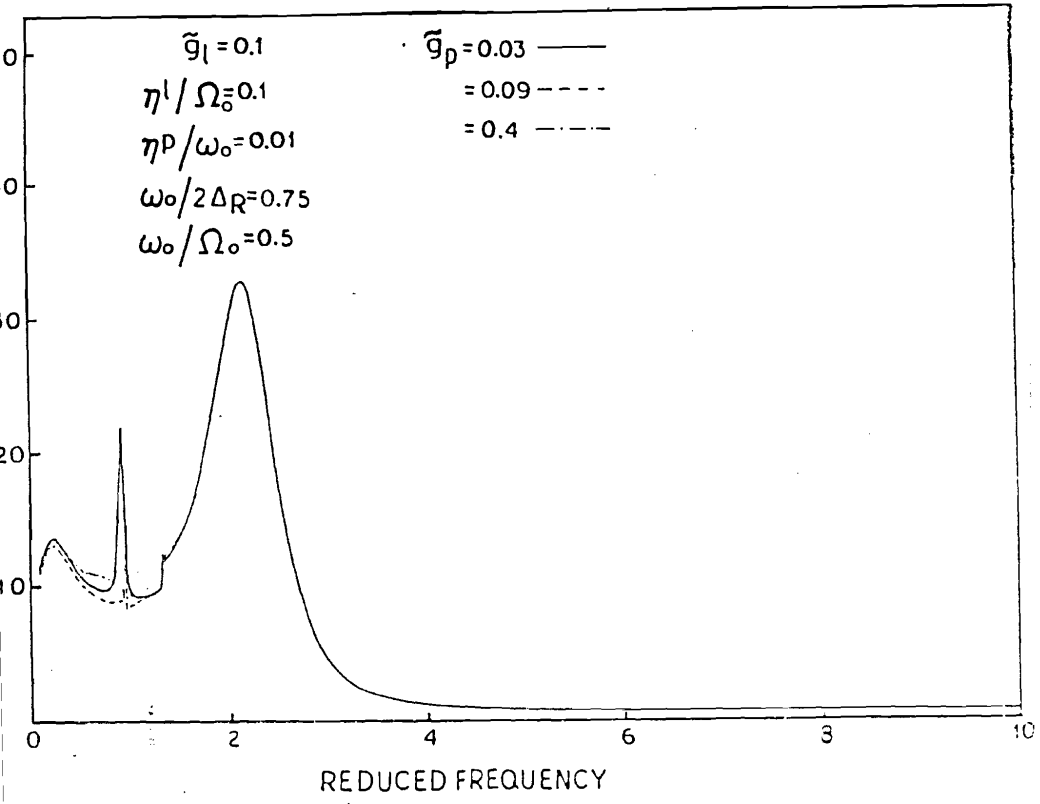
$\tilde{g}_l = 0.1$
$\eta^l / \Omega_o = 0.1$
$\eta^p / \omega_o = 0.01$
$\omega_o / 2\Delta_R = 0.75$
$\omega_o / \Omega_o = 0.5$
$\tilde{g}_p = 0.03$
$= 0.09$
$= 0.4$
0
2
4
6
3
10
REDUCED FREQUENCY

Fig.7

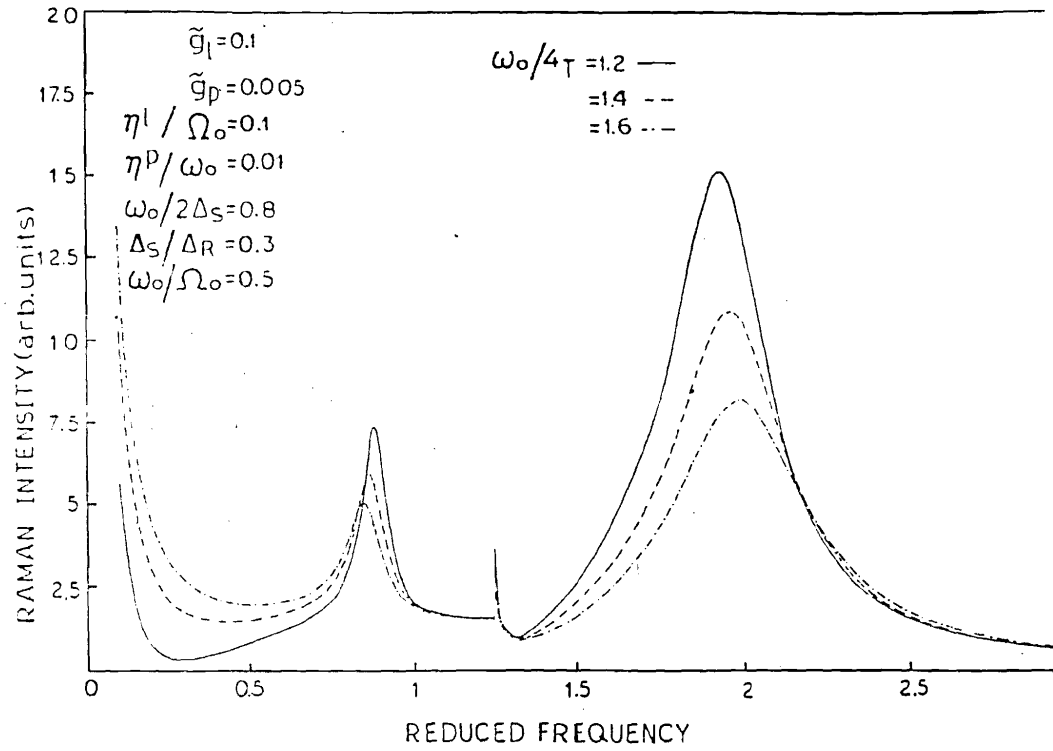
$\tilde{g}_l = 0.1$
$\tilde{g}_p = 0.005$
$\eta^l / \Omega_o = 0.1$
$\eta^p / \omega_o = 0.01$
$\omega_o / 2\Delta_S = 0.8$
$\Delta_S / \Delta_R = 0.3$
$\omega_o / \Omega_o = 0.5$
$\omega_o / 4_T = 1.2$
$= 1.4$
$= 1.6$
RAMAN INTENSITY (arb.units)
20
17.5
15
12.5
10
7.5
5
2.5
0
0.5
1
1.5
2
2.5
REDUCED FREQUENCY

Fig.8

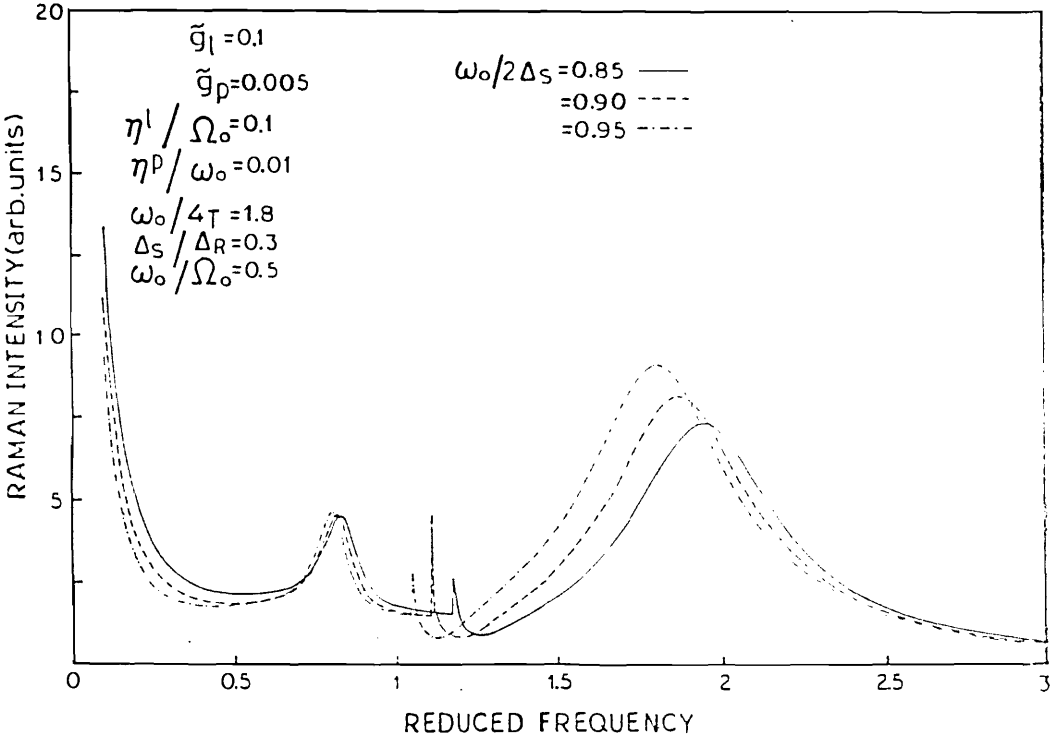
$\tilde{g}_l = 0.1$
$\tilde{g}_p = 0.005$
$\eta^l / \Omega_o = 0.1$
$\eta^p / \omega_o = 0.01$
$\omega_o / 4_T = 1.8$
$\Delta_S / \Delta_R = 0.3$
$\omega_o / \Omega_o = 0.5$
$\omega_o / 2\Delta_S = 0.85$
$= 0.90$
$= 0.95$
RAMAN INTENSITY (arb.units)
REDUCED FREQUENCY
0
0.5
1
1.5
2
2.5
3
5
10
15
20

Fig.9

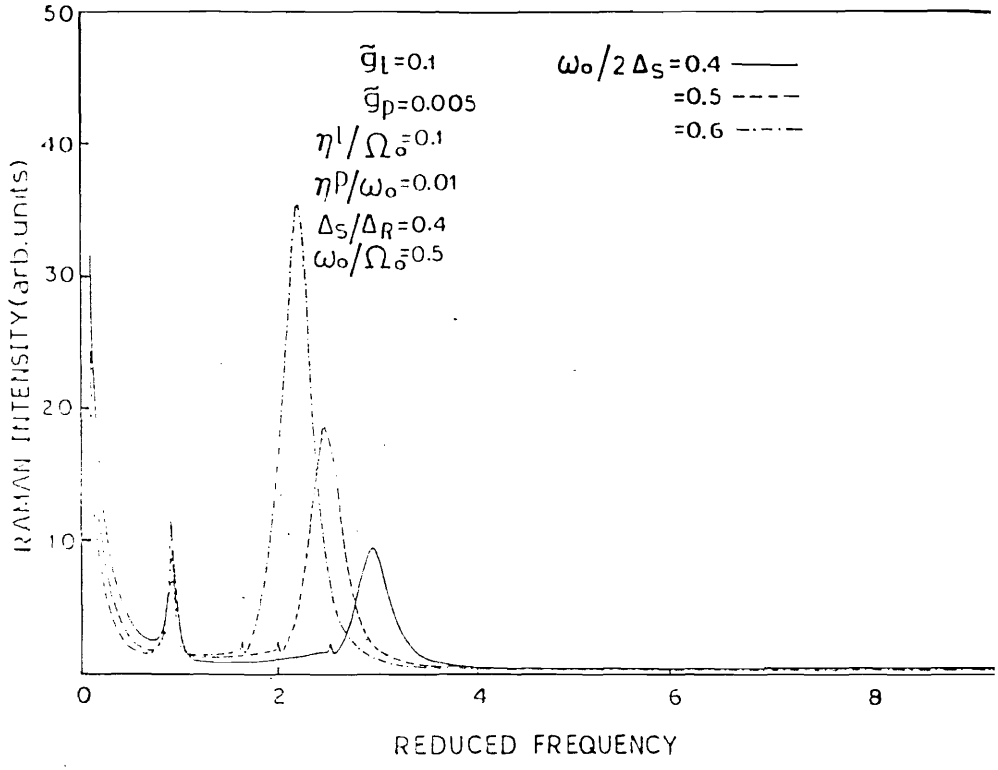
$\tilde{g}_l = 0.1$
$\tilde{g}_p = 0.005$
$\eta^l / \Omega_o = 0.1$
$\eta^p / \omega_o = 0.01$
$\Delta_S / \Delta_R = 0.4$
$\omega_o / \Omega_o = 0.5$
$\omega_o / 2\Delta_S = 0.4$
$= 0.5$
$= 0.6$
RAMAN INTENSITY (arb.units)
REDUCED FREQUENCY
0
2
4
6
8
10
20
30
40
50

Fig.10

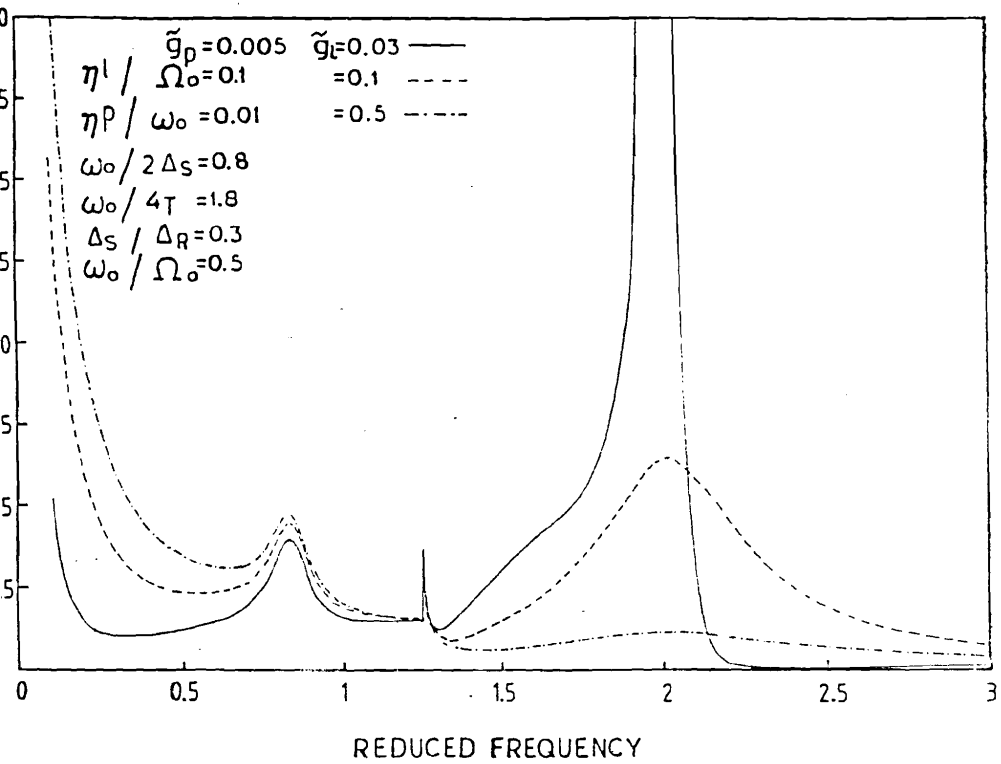
$\tilde{g}_p$ =0.005 $\tilde{g}_l$=0.03
$\eta^l / \Omega_o$=0.1 =0.1
$\eta^p / \omega_o$ =0.01 =0.5
$\omega_o / 2\Delta_s$=0.8
$\omega_o / 4_T$ =1.8
$\Delta_s / \Delta_R$=0.3
$\omega_o / \Omega_o$=0.5
0
0.5
1
1.5
2
2.5
3
REDUCED FREQUENCY

Fig.11

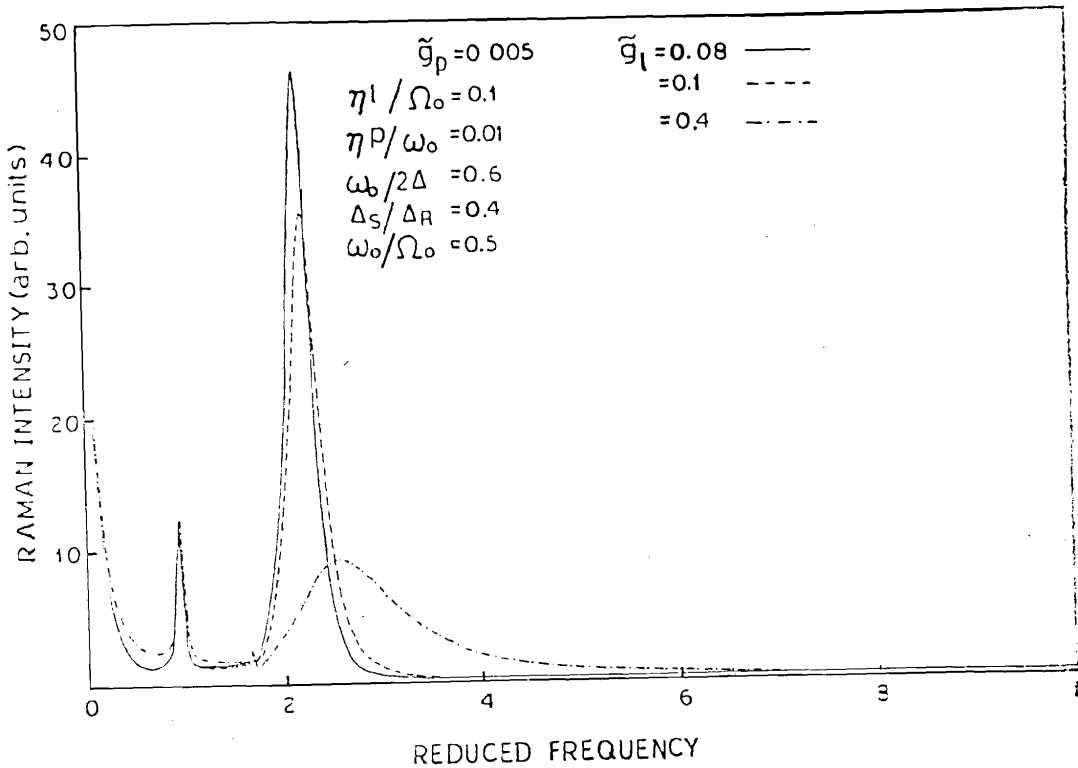
$\tilde{g}_p$ =0 005
$\tilde{g}_l$ =0.08
=0.1
=0.4
$\eta^l / \Omega_o$ = 0.1
$\eta^p / \omega_o$ =0.01
$\omega_b / 2\Delta$ =0.6
$\Delta_s / \Delta_R$ =0.4
$\omega_o / \Omega_o$ =0.5
RAMAN INTENSITY (arb. units)
50
40
30
20
10
0
2
4
6
8
REDUCED FREQUENCY

Fig.12

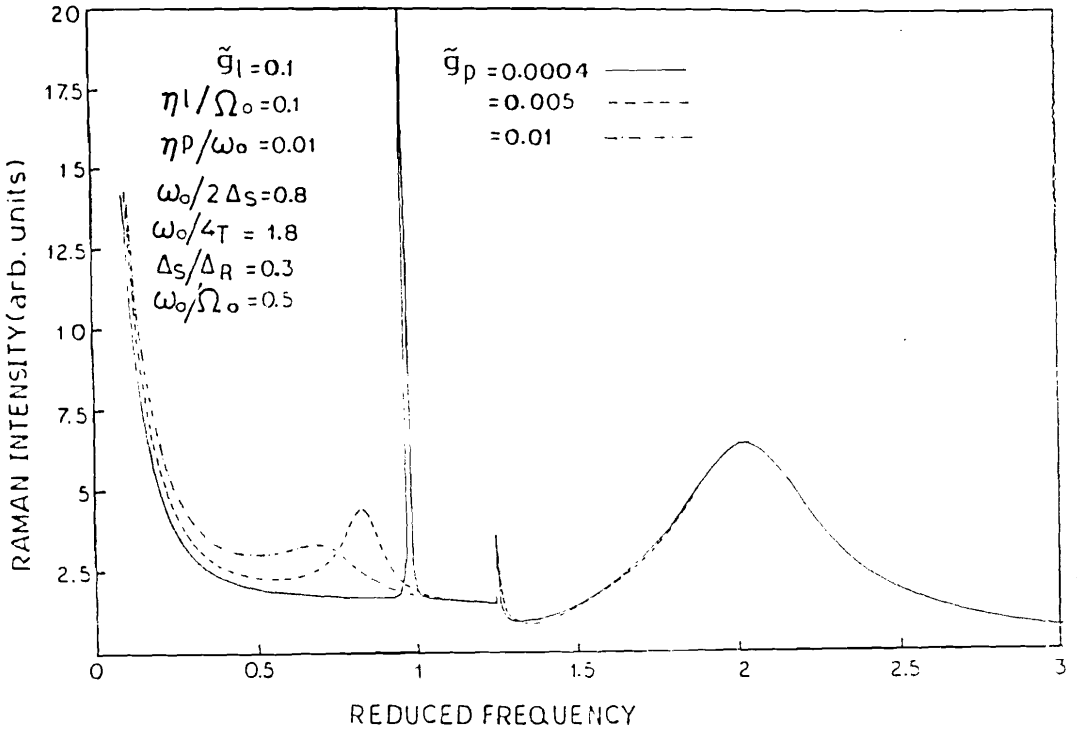
$\tilde{g}_l = 0.1$
$\eta^l/\Omega_o = 0.1$
$\eta^p/\omega_o = 0.01$
$\omega_o/2\Delta_S = 0.8$
$\omega_o/4_T = 1.8$
$\Delta_S/\Delta_R = 0.3$
$\omega_o/\Omega_o = 0.5$
$\tilde{g}_p = 0.0004$
$= 0.005$
$= 0.01$
RAMAN INTENSITY (arb. units)
REDUCED FREQUENCY

Fig 13

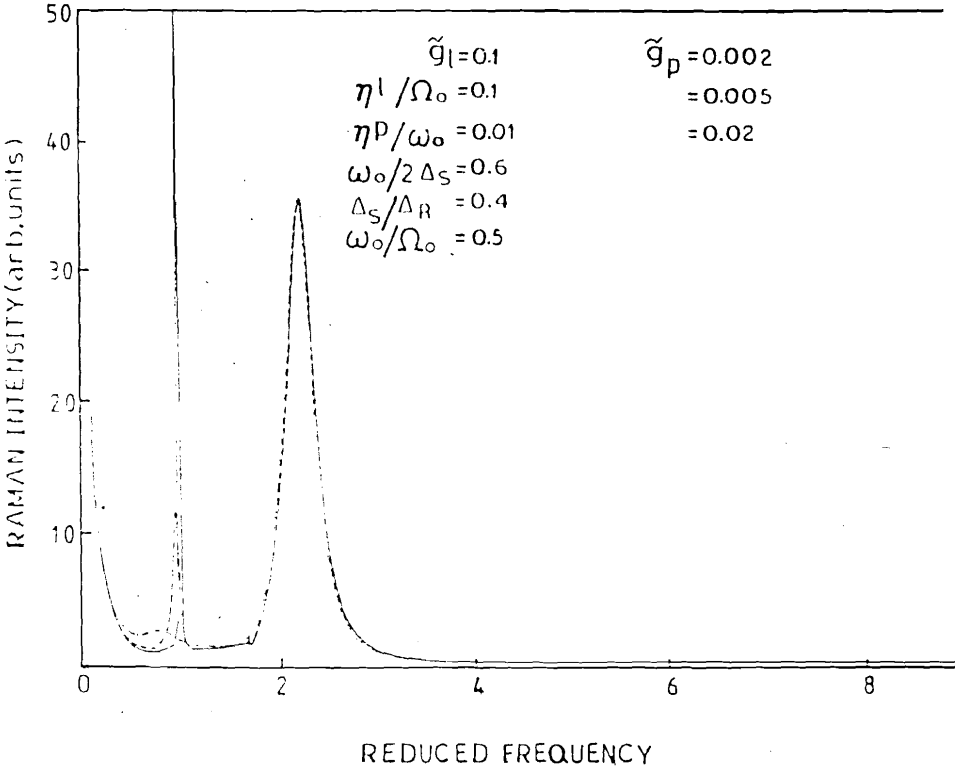
$\tilde{g}_l = 0.1$
$\eta^l/\Omega_o = 0.1$
$\eta^p/\omega_o = 0.01$
$\omega_o/2\Delta_S = 0.6$
$\Delta_S/\Delta_R = 0.4$
$\omega_o/\Omega_o = 0.5$
$\tilde{g}_p = 0.002$
$= 0.005$
$= 0.02$
RAMAN INTENSITY (arb. units)
REDUCED FREQUENCY

Fig.14